

©SHUTTERSTOCK.COM/BAKKMESTERKE

Quantum Dot Lasers and Amplifiers on Silicon

Recent advances and future developments.

A SELF-ASSEMBLED QUANTUM dot (QD) gain medium has multiple favorable material properties over conventional quantum well (QW) structures and bulk materials, including a large tolerance for material defects, reduced reflection sensitivity, nearly zero line-width enhancement factor, low transparency current density, high temperature operation, and ultrafast gain dynamics useful for semiconductor mode-locked lasers and amplifiers. Here, we review the recent advances in the field of QD lasers and amplifiers with a focus on the direct growth on silicon (Si). Si photonics has found widespread application, particularly for high volume applications and for co-integration with CMOS electronics.

YATING WAN, JUSTIN NORMAN, SONGTAO LIU, ALAN LIU, AND JOHN E. BOWERS

Digital Object Identifier 10.1109/MNANO.2020.3048094
Date of current version: 3 February 2021

We start with an overview of the field, followed by a summary of the device performance as well as the fundamental physics basis for the improved response. A subset of recent advances includes 119 °C continuous wave (CW) lasing, near zero linewidth enhancement factors, isolator-free stability, extrapolated lifetimes of more than 100 years at 35 °C, a CW submilliamp threshold in microscale ring laser cavities, high on-chip gain (39 dB) amplification, 4.1-Tb/s transmission using mode-locked lasers with a record-low timing jitter of 82.7 fs, and tunable lasers with more than 45-dB side-mode-suppression ratio (SMSR) and a 16-nm tuning range. Significant progress has been made in the last decade, making the commercialization of QD technology likely for practical III-V/Si photonics.

BACKGROUND

The first demonstration of self-assembled QD lasers dates back to the early 1990s and was predominantly motivated by the theoretical advantages of a gain medium with a zero-dimensional density of states (DOSs) [1]. However, experimental QD-based laser characteristics lagged behind theoretical expectations and were inferior to that of QW lasers [2]. Since then, intense studies have been conducted to analyze the fundamental physics of the phenomena taking place in the dots and how they interrelate with the laser performance [3], [4].

A real breakthrough occurred with the demonstration of the self-assembled Stranski–Krastinow growth of indium arsenide/gallium arsenide (InAs/GaAs) QD lasers [5]–[7]. Compared to the synthesis method based on electron-beam lithography patterning [8], focused ion beam etching [9], and selective-area growth [10], the Stranski–Krastinow growth mode relies on a strain relaxation-driven process, where islands form spontaneously above a certain critical thickness to relieve the mismatch strain and can easily yield a high density of mid 10^{10} cm⁻² QDs in a single layer. The 3D islands can be grown to be dislocation free and coherent with the surrounding lattice, with all of the dimensions being smaller than the de Broglie wavelength of electrons and holes. This gives rise to

fully quantized electron and hole states with delta function-like DOSs and quantization energies on the order of $k_B T$ at room temperature.

QD lasers fabricated with this approach confirmed the predicted ultralow threshold current density (J_{th} 120 A/cm²) and low temperature dependency ($T_0 = 350$ K at 77 K) [11]. Intense worldwide efforts have been devoted to further develop control over material growth and device fabrication. This has led to improved QD laser performance that outperforms the best values for QW lasers. In terms of J_{th} , InAs/GaAs QD lasers hold the lowest values of 10 A/cm² with a record-low internal loss of 0.25 cm⁻¹ [12]. The historical trend of J_{th} in semiconductor lasers has been discussed in [13], [14], demonstrating the lower ultimate values of J_{th} by reducing the dimensionality of the active region from double heterostructures to QWs and, in the ultimate case, QDs.

In terms of temperature stability, nearly complete temperature insensitivity of the threshold current has been achieved in a range of 5–70 °C [15]. Commercially available 1.3- μ m QD lasers now produce high-temperature CW operation up to 220 °C [16]. An optical interposer with QD lasers has achieved error-free data links at 20 Gb/s and a high bandwidth density of 19 Tbps/cm² up to 125 °C [17]. A low linewidth enhancement factor has been demonstrated, which results in low reflection sensitivity behavior [18].

In addition to lasers, QDs have been extensively investigated for a range of devices, including photodiodes, amplifiers, and solar cells, and for a range of applications, including data communications, optical memory, space applications, and so on. The fact that the QDs can be embedded in a semiconductor matrix enables the fabrication of a very wide range of QD-based semiconductor devices. QD photodiodes are able to detect light in the mid infrared, far infrared, and terahertz frequencies with a low dark current, an intrinsic sensitivity to normal incidence light, much longer carrier lifetime, and a higher operating temperature due to the reduced electron–phonon scattering [19]–[22].

While commercial mercury cadmium telluride detectors and QW infrared photodetectors require cryogenic cooling to reduce thermal noise and obtain a reasonable signal-to-noise ratio (SNR), QD infrared photodetectors can achieve room temperature operation with a peak responsivity of 5.3 A/W and a comparably high detectivity of 6×10^8 cmHz^{1/2}/W [23]. For telecom wavelength detection, mainstream InGaAs and germanium (Ge) photodiodes have a typical dark current density in the order of 5×10^{-5} and 1×10^{-2} A/cm², respectively [24], [25]. As a comparison, more than two orders of magnitude lower dark current densities have been achieved with QD materials in the O-band (3.5×10^{-7} A/cm²) [26] and C-band (3.3×10^{-7} A/cm²) [27].

Due to the fast carrier dynamics, low confinement factor, and decoupling of gain and phase dynamics, QD semiconductor optical amplifiers (SOAs) have exceptional device performance rivaling what has been achieved through any other existing optical amplifiers [28]. Native substrates have demonstrated more than 25 dB gain, 20-dBm 3-dB saturation output power, and 90-nm amplification bandwidth, and smaller than 5-dB noise figures [29]. An almost three-fold increase of cross-gain modulation bandwidth has been achieved compared to a commercially available QW counterpart [30]. QD-based solar cells offer high power conversion efficiency with the additional sub bandgap transition to absorb otherwise wasted lower energy photons [31]. A relative efficiency improvement of 3.6% over the control cell, or an absolute efficiency improvement of 0.5%, has been demonstrated in QD solar cells with a short circuit current density of 0.02 mA/cm²/QD layer and an open circuit voltage loss of 50 mV [32]. A comprehensive review of QD-based device performance and related applications is given in excellent review works [13], [14], [19].

Among all of the mentioned device applications, the most prominent one is near-infrared QD lasers. In addition to the significantly reduced J_{th} , high-temperature operation, reduced reflection sensitivity, and narrow linewidth

discussed, the insensitivity of QDs to defects allows for the epitaxial integration of lasers on Si, providing a much lower barrier to entry for Si photonics. This is extremely important for the development of optoelectronic integration with CMOS, which has been limited by the lack of availability of monolithic Si-based light sources.

Reviews of various approaches to using direct epitaxial growth to integrate InAs/GaAs QD lasers for Si photonics applications can be found in [33]–[41]. Research in [33] contains results up to 2009 and has a laser operation wavelength up to 1.05 μm . Results in [34] go up to 2015 and showcase the direct comparison with similar QW lasers grown on Si. Device results in [35]–[37] are summarized up to 2019 and focus on the 1.3- μm wavelength. Discussions in [38], [39] indicate how QD gain medium is utilized for circumventing crystal defects during III-V/Si heteroepitaxy as well as for scaling to ultrasmall dimensions in microcavities. Research in [40] presents insights into the correlations between QD device characteristics and crystalline quality of the epitaxial template structures on Si. The focus of [41] is on the epitaxial growth method of various III-V QD lasers with an emphasis on developing a CMOS-compatible epitaxial platform on (001) Si, where III-V growth can be scaled up to 300-mm Si wafers.

LOWER THRESHOLD

A key driver in developing QD lasers is the ultralow threshold current density (J_{th}) [1]. The DOS and gain spectra become narrower when decreasing the dimensionality of the laser active region. This requires fewer states to be filled to make the active region transparent, leading to a reduced transparency current and, consequently, a reduced threshold current. Theoretical studies suggest that the minimum J_{th} , neglecting any current leakage, is merely 2 A/cm^2 given a typical dot size distribution of 10%, a dot area density of $4 \times 10^{10} \text{ cm}^{-2}$, and a QD carrier decay time of 2 ns [42]. This is more than one order of magnitude lower than that of the best-reported values in QW lasers ($45 \text{ A}/\text{cm}^2$) [43].

A significant reduction of J_{th} in QD lasers was achieved by incorporating a

dot-in-a-well (DWELL) strain-reducing design and by applying p-type doping in the QD active region. The DWELL design places an InAs QD layer in a thin (typically 5–10 nm) $\text{In}_x\text{Ga}_{1-x}\text{As}$ ($x \approx 10\text{--}30\%$) QW, giving rise to improved carrier capture, increased dot density, and thus increased material gain. With p-type doping, the extra holes reduce the carrier density required to achieve a sufficiently large quasi Fermi-level separation. These combined effects translate into a significant improvement in material gain and a much-reduced laser transparency point.

In 2009, the prophecy of low J_{th} became true, with the smallest value of J_{th} attained by QDs being merely 10 A/cm^2 , surpassing any type of semiconductor lasers [12]. The historical development of QD lasers on Si [44], [45] follows a similar learning curve as that of QD lasers grown on a native GaAs substrate [13], [14]. A record-low threshold current density of 62.5 A cm^{-2} has been achieved with a $3,200 \times 50 \mu\text{m}^2$ broad area laser [45], and a record-low threshold current of 6.2 mA has been demonstrated with narrow ridge waveguide geometry [46].

For the ridge QD lasers grown on a Si substrate, a clear trend of lower threshold currents was observed when decreasing the laser ridge widths [Figure 1(a)], demonstrating negligible sidewall recombination effects stemming from excellent lateral carrier confinement in QD lasers. This spawned intense interest to explore a new size regime for microcavity lasers, which are motivated by the quest for reducing the “footprint” of photonic components, thereby affording a larger scale of on-chip integration [38], [48]–[53]. Typically, QW-based microcavity devices experience serious sidewall scattering and recombination as the resonator size is reduced to tens of microns. This issue becomes more prominent with the exposure of the active region to the sidewall, where a deeply etched waveguide is required to obtain minimal bending losses. In QDs, the in-plane diffusion length is reduced to $\sim 0.5 \mu\text{m}$ as opposed to that of several microns in QWs [54]. Therefore, QDs efficiently reduce the sensitivity to recombination at device sidewalls and other surface defects in a similar way as they reduce the sensitivity to dislocations.

Under CW optical pumping, QD photonic crystal membranes grown on a native substrate have yielded an ultralow threshold of 25 nW and a high spontaneous emission factor of 0.85 [55]. QD photonic crystal lasers have exhibited single-mode operation with an ultralow threshold of $\sim 0.6 \mu\text{W}$ and a large spontaneous emission coupling efficiency up to 18% [51]. Meanwhile, through direct heteroepitaxy on a Si substrate, subwavelength QD microdisk lasers as small as 1 μm in diameter were achieved with a threshold of 35 μW and a spontaneous emission factor of 0.3 [56].

Under electrical injection, QD microring lasers directly grown on Si have achieved submilliamp thresholds by significantly improving the spontaneous emission efficiency and modifying the electromagnetic field distribution. This is one degree of magnitude lower than the best edge-emitting QD lasers. As expressed in Figure 1(b), for a series of QD microring lasers with different outer ring radii and a constant ring waveguide width of 4 μm , a monotonical decrease of threshold current is observed when reducing the ring diameter. An ultralow threshold current of $\sim 0.5 \text{ mA}$ is obtained for the smallest dimension with a radius of 5 μm and a ring waveguide width of 3 μm .

While the high aspect ratio of sidewall/active region volume of the microring structure and defects arising from the III-V/Si heteroepitaxy might induce a large J_{th} , the J_{th} of QD microrings can be reduced as low as 306 A/cm^2 by properly managing the threading dislocation density (TDD) of the GaAs buffer layer and by optimizing the etching sidewall [57]. As illustrated in Figure 1(d) and (e), an atomic force microscopy (AFM) image of QDs was drawn to scale with a plan-view ECCI scan. Most device areas are “defect-free” considering the four magnitudes higher density of QDs ($6 \times 10^{10} \text{ cm}^{-2}$) versus the TDDs ($7 \times 10^6 \text{ cm}^{-2}$) and the small footprint of the microring devices. As a result, QD microrings directly grown on Si can be largely unperturbed relative to their native substrate counterparts, which is ideal for ultradense photonic integration with low power consumption.

HIGHER TEMPERATURE STABILITY

In addition to the ultralow J_{th} , high-temperature stability is another equally important feature expected for QD lasers.

A full 3D carrier confinement should restrict charge carriers exclusively to the states involved in lasing, independent of temperature [1]. However, real QDs

usually have several excited states that may be thermally occupied. The holes are inherently much closer in energy to each other due to the heavier effective

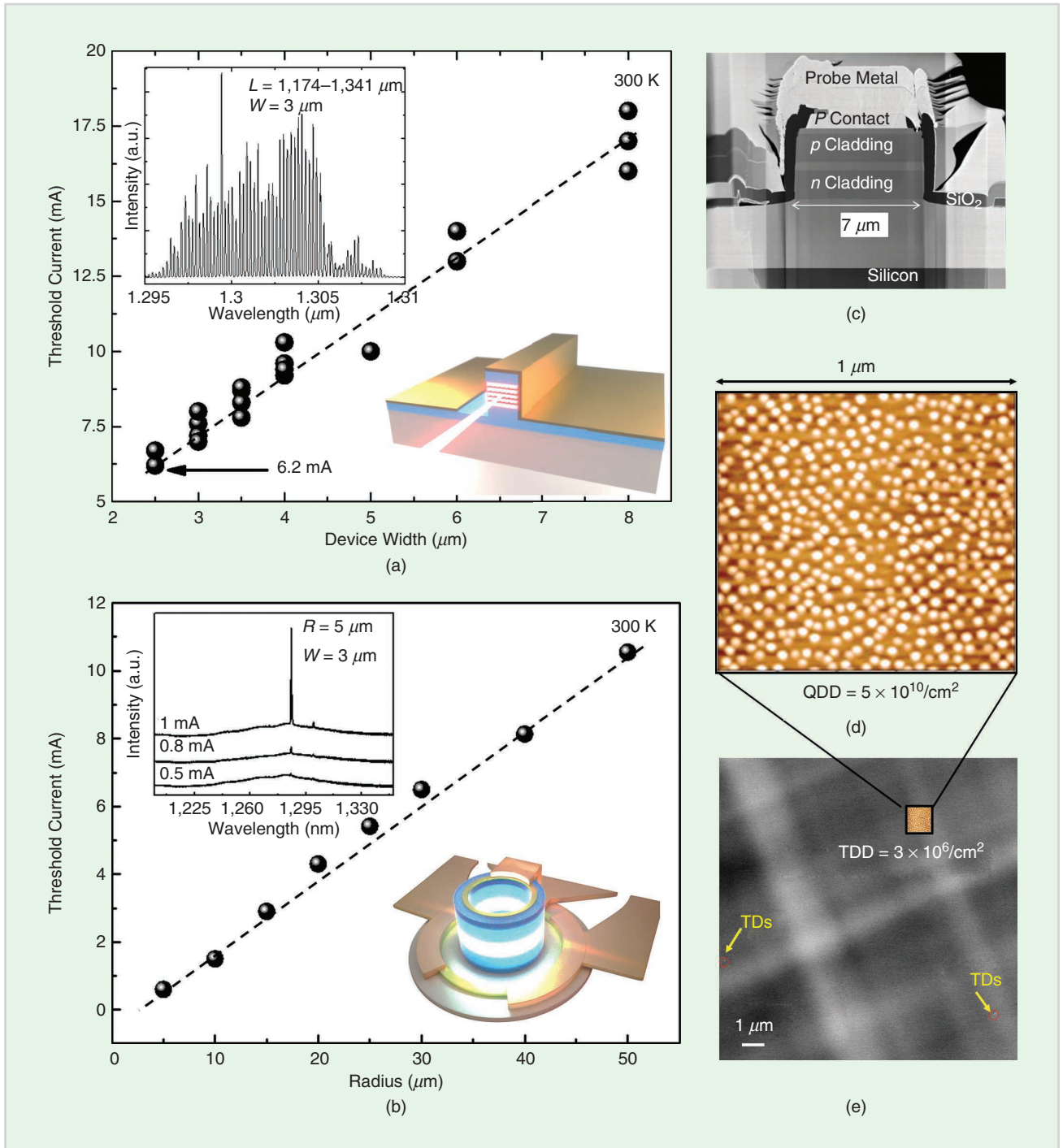


FIGURE 1 The threshold performance for QD laser directly grown on a (001) Si substrate. (a) The threshold current versus device width for QD ridge lasers with as-cleaved facets. The dashed line represents a linear fit. Upper inset: the high-resolution lasing spectra taken at two times the threshold. Lower inset: a schematic diagram of the device. (b) The threshold current versus device width for QD microring lasers. The dashed line represents a linear fit. Upper inset: the high-resolution lasing spectra for various pump currents. Lower inset: a schematic diagram of the device. (c) A cross-sectional scanning electron microscopy (SEM) image of the QD ridge lasers with as-cleaved facet. (d) An AFM image of uncapped InAs QDs. (e) Plan-view electron channeling contrast imaging (ECCI) showing only two TDDs in the GaAs/Si template over a $14.5 \mu\text{m} \times 14.5 \mu\text{m}$ field of view. Inset: An AFM image of the uncapped quantum dots scaled to the size of the ECCI image to illustrate the high ratio of dots to dislocations [46], [47].

mass compared to electrons. There is a valence band separation of around 10 meV between the ground state and first excited state compared to that in the conduction band (~70 meV) [16].

With increased temperature, the thermal injection of charge carriers from the ground state to the excited states can cause exponentially increasing threshold current, where the thermal spread of holes acts as the main mechanism for reduced temperature stability. P-type modulation doping to reduce J_{th} is also pivotal for improving temperature stability [58]. With higher p-doping, the temperature dependence of the gain is increasingly set by the electron energy levels that are widely spaced in

energy. This gives rise to a significantly increased temperature stability.

Commercially produced 1.3- μm QD lasers are available for operation at extremely high temperatures (150–200 °C) [59]. Temperature invariant operation ($T_0 = \infty$) in a range of 5–70 °C [15], with a maximum CW operating temperature up to 220 °C [16], and an athermal optical interposer with error-free data links at 20 Gb/s at 125 °C [17] have been demonstrated. For QD lasers grown on Si substrates, CW lasing up to 119 °C and pulsed operation up to 130 °C have been reported [60]. A five times improvement in characteristic temperature (T_0) is achieved by p-type modulation doping with a hole concentration of

$5 \times 10^{17} \text{ cm}^{-3}$, compared to an undoped QD active region [49].

A detailed analysis of the importance of p-doping for high-temperature stability revealed consistent behaviors with previous studies of 1.3- μm QD lasers grown on native GaAs substrates, indicating that the high characteristic temperatures of QD lasers directly grown on Si are barely perturbed relative to their native substrate counterparts [61]. Even for microcavity lasers where the high aspect ratio of sidewall/active region volume can seriously deteriorate the temperature performance, a CW temperature up to 100 °C is demonstrated with a T_0 of 197 K between 10 and 50 °C and of 55 K between 60 and 100 °C, as illustrated in Figure 2 [47], [62].

DEFECT INSENSITIVITY

Motivated by the quest to achieve monolithically integrated Si-based laser sources, research has been conducted since the 1980s to grow QW-based lasers directly on Si. Since the first demonstration [63], substantial improvements have been achieved in terms of J_{th} (214 A/cm²) [64], light output power (400 mW/facet) [65], and external quantum efficiencies (87%) [66] that are comparable to those obtained on native GaAs substrates. However, early aging tests showed a very short device lifetime of a few seconds, with a rapid increase in threshold [67]. Even with an ultralow TDD of $2 \times 10^6 \text{ cm}^{-2}$ obtained through a time-consuming growth of a 10- μm thick Ge/GeSi/Si buffer, CW lifetime was merely improved to around 4 h [68].

Degradation mechanisms of the laser failures have been heavily researched, and dark line defects (DLDs) initiated by the presence of TDDs are identified to be the most critical mechanism. Substantial efforts have been made to control defect formation in monolithic III-V heteroepitaxy on Si via strained interlayers, thermal cycling, and selective area growth [69]–[74]. However, further lowering of the TDD below 10^6 cm^{-2} is difficult. Since the interaction between dislocations is the only mechanism to filter out dislocations in bulk films, with such a low TDD, the possibility of two dislocations meeting

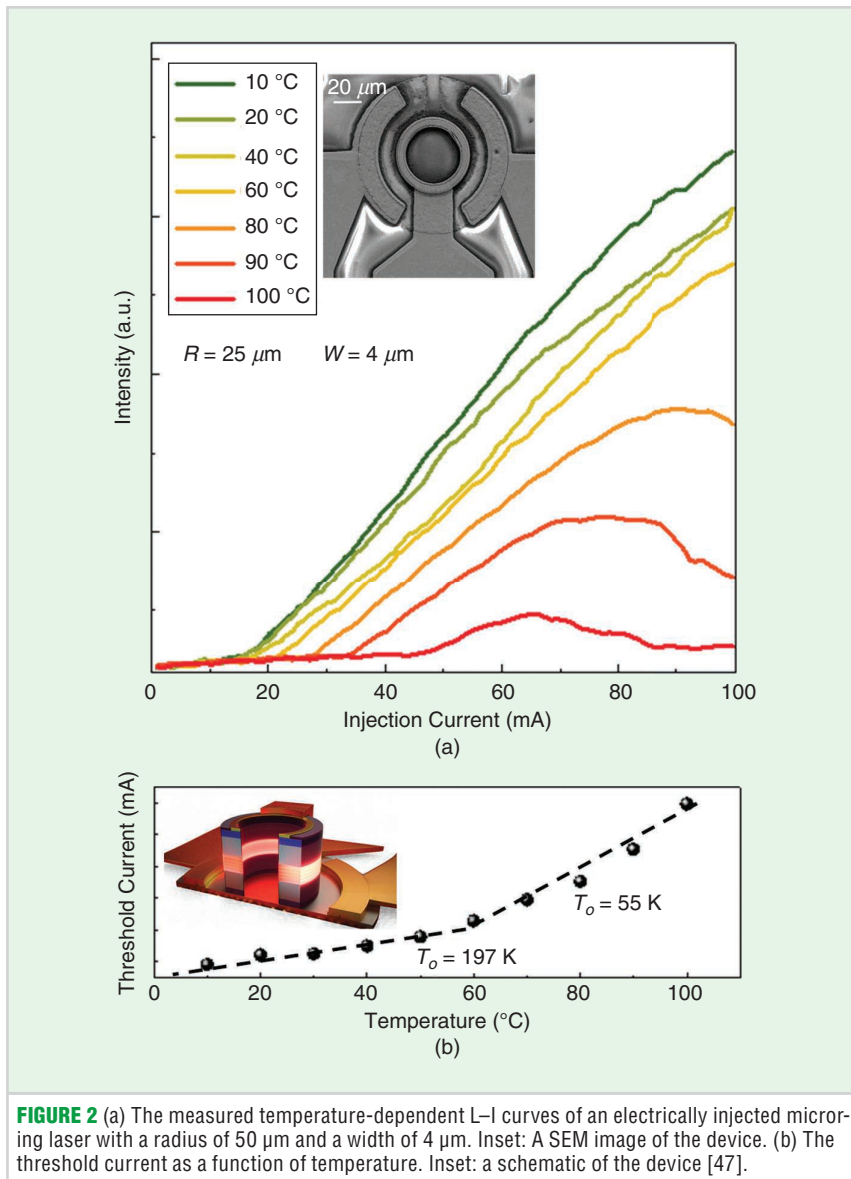


FIGURE 2 (a) The measured temperature-dependent L-I curves of an electrically injected microring laser with a radius of 50 μm and a width of 4 μm . Inset: A SEM image of the device. (b) The threshold current as a function of temperature. Inset: a schematic of the device [47].

each other to annihilate is exceedingly low [75]. As a result, defect-free III-V/Si or even defect levels comparable to that of state-of-the-art III-V wafers ($103\text{--}104\text{ cm}^{-2}$) is never available.

In the end, even one dislocation can result in the failure of a QW device, and the most prolonged lifetime reported among all GaAs-based QW lasers on Si is only around 200 h after more than a decade of research [76]. The historical development of the J_{th} and the device lifetime for QW-on-Si and QD-on-Si lasers is depicted in Figure 3. Despite the impressively low J_{th} (269 A/cm^2), GaAs QW lasers failed to achieve sufficiently long lifetimes to be fully considered for commercial applications.

Meanwhile, ever since the first demonstration of QD lasers grown on Si [77], the performance of QD lasers has quickly surpassed that of QWs. While the lowest J_{th} of QDs (62.5 A/cm^2) [45] is only four times smaller than that of QWs (269 A/cm^2) [68], the first aging test of QD lasers exhibit more than 2,700 h of CW operation with no catastrophic failures at $30\text{ }^\circ\text{C}$ and an extrapolated mean time to failures (doubling the initial threshold) up to 4,600 h [78]. This is orders of magnitude longer than any previous lifetime test of III-V lasers epitaxially grown on a Si substrate with a QW active region. By reducing the TDD from 3×10^8 to $7 \times 10^6\text{ cm}^{-2}$, commercially promising extrapolated lifetimes of more than $10 \times 10^6\text{ h}$ can be achieved despite the fact that the TDD is still two orders of magnitude higher than that of the native substrates (Figure 4) [79].

For QD lasers, one dislocation generated from III-V/Si heteroepitaxy affects a few dots. With a typical TDD on the order of 10^6 cm^{-2} in optimized buffers and a typical QD density of $5 \times 10^{10}\text{ cm}^{-2}$, the possibility of charge carriers recombining radiatively within a dot before recombining nonradiatively with a dislocation is very high. By reducing the amount of nonradiative recombination at dislocations, QDs limit the extent of recombination-enhanced dislocation climb in the material, which is the most critical driving force for the evolution of DLDs responsible for rapid device failures [80]. Furthermore, QDs act to stiffen the

lattice and make the material more resistant to defect propagation [81]. This gives QDs far less sensitivity to the presence of defects than QWs.

In aging tests conducted at Intel Corporation, QD lasers were stressed at $35\text{ }^\circ\text{C}$

[Figure 5(a)] and $60\text{ }^\circ\text{C}$ [Figure 5(b)] under CW operation, with driving currents set at two times the initial threshold current. At room temperature ($35\text{ }^\circ\text{C}$), almost no degradation was observed after the initial 200 h of aging, and only an 8%

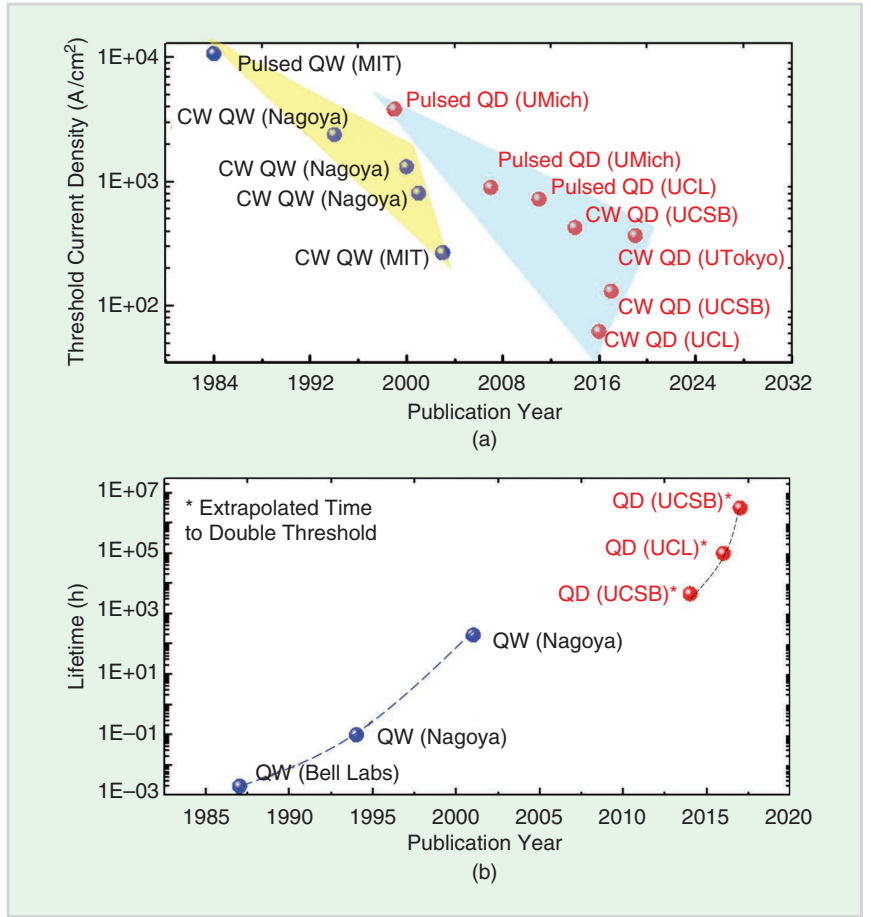


FIGURE 3 The historical development of the (a) threshold current densities and (b) device lifetime. MIT: Massachusetts Institute of Technology; UMich: University of Michigan; UCL: University College London; UCSB: University of California Santa Barbara; UTokyo: University of Tokyo.

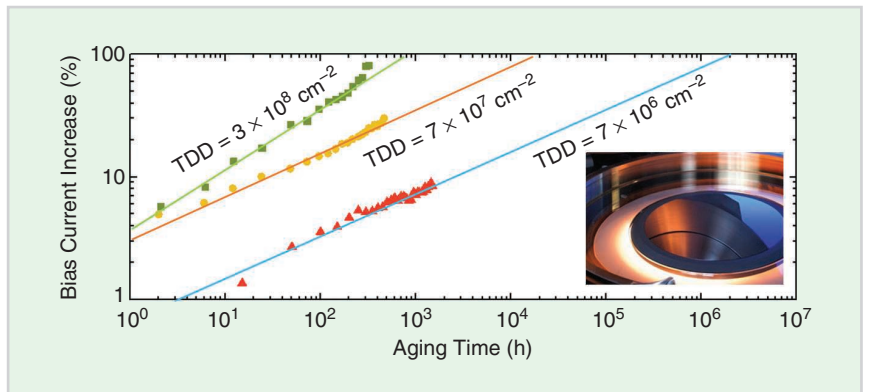


FIGURE 4 The extrapolated mean-time-to-failure, defined as a doubling of the threshold current, versus aging time for lasers with varying dislocation density. Inset: the 300-mm GaP/Si (001) on-axis wafer commercially available from NAsP_{III/V} GmbH.

decrease in the slope efficiencies occurred during the entire 4,000 h aging period. This leads to extrapolated lifetimes of more than 10^7 h for all of the lasers being aged. At an elevated temperature of 60 °C, which is important for practical applications in data centers or on-chip optical interconnects, the extrapolated lifetimes are more than 65,000 h. More research is ongoing to understand the device lifetime behavior and improve reliability [82]–[84].

In addition to the advantages of reduced sensitivity to dislocations, the use of QDs in place of QWs offers reduced sensitivity to thermal fluctuations and radiation damage. Similar to the mechanisms of dislocation insensitivity, the effects of the 3D quantum confinement in QDs significantly reduced the likelihood of carrier nonradiative recombination at radiation-induced defect centers. As a result, the impact of high-energy radiation on the active layers is less likely to decrease the material efficiency. Photoluminescence emission from equivalent InGaAs/GaAs QW and QD structures have been compared after controlled irradiation with 1.5-MeV proton fluxes [85]. A two orders of magnitude increase in radiation hardness has been measured in QDs compared

to that of QWs of the same composition and placed at the same depth in the structure. The improved radiation hardness translates into the superior performance of irradiated QD lasers [86], enabling the successful application of QDs in spaceborne applications and metrology that require stringent radiation hardness standards.

To fully exploit the relative defect immunity of QD lasers for future laser growth and processing on full-size Si wafers as well as the relative radiation immunity of QD lasers for applications in space and other harsh environments, extensive research efforts have been conducted to explore the physical mechanisms responsible for the degradation of 1.3- μm InAs QD lasers grown on Si [87]. QDs can efficiently confine carriers and prevent defect reactions when devices are stressed at low current densities or low energy radiation. At high stressed conditions, carriers first recombine on the excited state and then escape out of the QDs and migrate to the QWs without being spatially confined. The lateral movement of carriers within the QW layers stimulates non-radiative recombination at dislocation/radiation-induced defect centers located in the proximity of the active region.

Consequently, degradation proceeds through recombination-enhanced defect reaction, causing performance degradation and, eventually, device failures.

The effect of proton bombardment in QD material has been quantified, and it has indicated that maximizing the QD density and capture probability per dot can efficiently increase the relative radiation immunity [88]. The effects of TDDs and the inclusion of p-modulation doping in the QD active region have been heavily explored [89], contributing to rapid progress in the reliability of the epitaxially grown QD on Si lasers. This improved capability of producing defect and radiation immunity of QD lasers indicates the great potential of QDs to be used in Si photonics applications and space applications.

LINewidth ENHANCEMENT FACTOR

The linewidth enhancement factor (LEF) is a key parameter in semiconductor lasers, determining the spectral linewidth, modulation-induced chirp, and sensitivity to optical injection or optical feedback [90]. The LEF (also termed the α -factor) describes the ratio of changes in the real part of the refractive index (n) of the laser medium with carrier density (N) to that of the imaginary part (n_i) with respect to the carrier density [91]. Mathematically, the α -factor can be re-expressed as a function of measurable parameters, as

$$\alpha_H = \frac{dn/dN}{dn_i/dN} = -\frac{4\pi}{\lambda} \frac{dn}{dg}$$

$$= -\frac{4n\pi}{\lambda^2} \frac{d\lambda}{dG_{\text{net}}}, \quad (1)$$

where λ is the wavelength, g is the gain, I is the injection current, and G_{net} is the variation of the net modal gain.

Therefore, the α -factor can be extracted by tracking the frequency shift of the longitudinal Fabry–Perot (FP) mode resonances to attain the value of the differential index and by measuring the net modal gain in the amplified spontaneous emission spectra to attain the value of the differential gain [92].

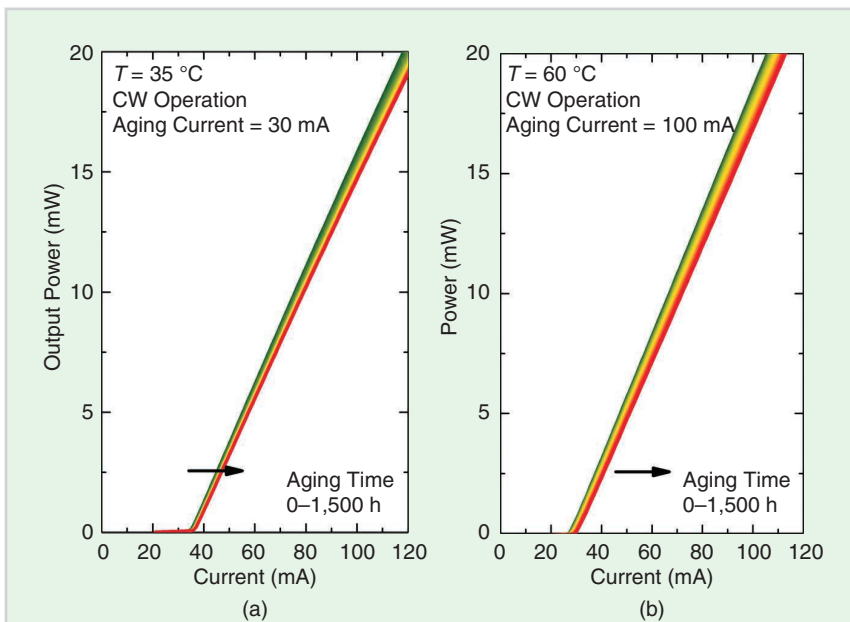


FIGURE 5 The L–I curves from (a) 30 °C and (b) 60 °C aging tests of QD lasers directly grown on Si. The driving currents were set at two times the initial threshold current.

From the definition, lower values of the α -factor can be obtained for materials with high differential gain and a symmetric gain spectrum. Due to the delta-like DOSs, the ideal inhomogeneously broadened gain spectrum of QD lasers assumes a highly symmetric Gaussian profile. Therefore, a near-zero α -factor can be expected for uniform QDs according to the Kramer–Kronig relationship, granted that the peak gain wavelength stays the same [92], [93]. In real cases, self-assembled QD lasers via the Stranski–Krastinow growth mode have a size variation in dots. The inhomogeneous broadening from the distribution of QD sizes and the higher excited state contributions result in a finite value of the actual α -factor.

Still, with highly uniform dot size distributions, QD lasers have yielded an ultralow α -factor of 0.13, independent of the temperature range being measured (288–308 K) [92], [94]. The possibility of pushing the α -factor into negative values has been envisioned with high dot uniformity and sufficient modulation p-doping [95]. Since the α -factor increases with higher injection, a negative α -factor at the subthreshold injection level makes it feasible to achieve a truly zero α -factor at a particular operating bias.

REFLECTION INSENSITIVITY

The advantages of a low α -factor are closely related to feedback susceptibility. In any integrated photonic system, unintentional reflections from various refractive index interfaces will be fed back into the laser cavity, inducing increased laser relative intensity noise (RIN), linewidth broadening, mode hopping, or even total coherence collapse. This is particularly detrimental to data communication systems as the increase in laser amplitude or phase noise increases the bit error rate (BER). Traditionally, external Faraday rotation-based optical isolators have been used to block the undesired reflections in photonic integrated circuits (PICs). The inclusion of optical isolators in the laser assembly increases the cost and footprint, complicates the packaging, and adds insertion loss.

Recently, Si-based on-chip isolators have been demonstrated with a maximum

isolation ratio of 32 dB and only 2.3 dB excess loss [96]. The compact integrated optical isolator with an electromagnet doesn't require precise positioning of a permanent magnet close to the chip, thus greatly reducing the packaging cost. However, their integration with lasers still adds extra process steps with increased cost, total chip/system size, and total loss within the system.

Therefore, isolator-free laser source operation is desirable to eliminate the copackaged/integrated optical isolator while still maintaining the required feedback tolerance. The strength of the feedback relative to a critical feedback level (f_{crit}) [91] is defined as the fractional proportion of the laser output power that can be externally reflected and fed back into the cavity before coherence collapse occurs:

$$f_{\text{crit}} = \frac{\tau_L \gamma^2}{16 C_e^2} \left[\frac{1 + \alpha^2}{\alpha^4} \right], \quad (2)$$

where τ_L is the cavity roundtrip time and $C_e = (1 - R/2\sqrt{R})$ is the coupling strength of the laser cavity to the external cavity, with a facet reflectivity of R [97].

From the scaling relations, the f_{crit} is closely related to the α -factor and the damping factor $\gamma = K f_r^2 + \gamma_0$, which is defined in terms of the K-factor, relaxation oscillation frequency, f_r , and damping offset, γ_0 . Lowering α from 2 (i.e., the state-of-the-art α for QWs) to 0.13 (i.e., the state-of-the-art α for QDs) can result in a factor of more than 11,000 times increase in the critical feedback level for coherence collapse. Together with the highly damped relaxation oscillations from larger K-factors (1 ns for QDs and 0.265 ns for QWs) [4], QD lasers exhibit more than 100,000 times increase (or 50 dB) in the critical feedback level, such that coherence collapse does not occur even with 90% of the light reflected back to the laser.

Figure 6 depicts the spectral evolution as a function of feedback level for both QD and QW lasers in the optical domain and the RF domain. QD lasers directly grown on Si show excellent insensitivity to optical perturbations, with only a slight red shift of the modal wavelength in the optical domain and no sign of nonlinear oscillations in the RF response. In comparison, the QW lasers

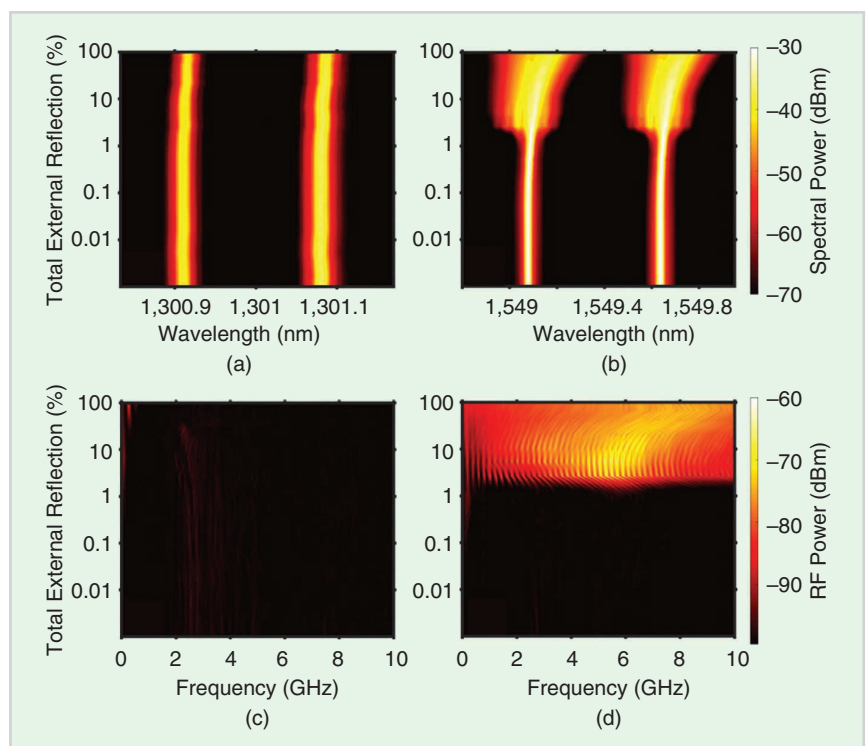


FIGURE 6 Optical spectra for (a) QD and (b) QW lasers as a function of the feedback level. The corresponding radio frequency (RF) spectra mappings for the (c) QD and (d) QW lasers. The lasers are biased at $3 \times I_{\text{th}}$, and the vertical axes are on a log scale. Figure from [94].

undergo coherence collapse with a strong broadening of the FP modes and intense chaotic oscillations in the RF domain at a feedback level of 1.7% [94]. This enables an aggregate data rate of more than 640 Gb/s using an array of QD distributed feedback (DFB) lasers from a chip without isolators to avoid a feedback effect in the system demonstration [98].

In addition to coherence collapse, optical feedback can increase RIN, which degrades the SNR and increases the BER. Since RIN is inversely proportional to the damping rate, the approximately five times higher K-factor in QDs relative to QWs leads to a much-reduced sensitivity [99]. Compared to heterogeneously integrated QW lasers, QD lasers show a nearly 20 dB reduced sensitivity to feedback with total system RIN below -140 dBc/Hz from 100 to 10 GHz [100]. At the system level, the use of on-chip QD lasers without optical isolation gives rise to a low power penalty of 1 dB at 5 Gb/s after a 12-km transmission distance [101], a penalty-free operation for BER < 10⁻¹² at 10 GHz external modulation with 100% (i.e., -7.4 dB) optical feedback [94], error-free operation at 25 Gb/s and more than 70 °C in a chip-scale Si-photonics optical transmitter [102], and negligible signal degradation by optical feedback within the transmitter for an optical input–output core [103].

Furthermore, researchers have found that the critical feedback level strongly depends on the ground-state-to-excited-state lasing threshold ratio. Stronger insensitivity to the optical feedback is expected by slowing the switching from the ground state to the excited state. Together with a low α -factor that can be achieved through high dot size uniformity, appropriate p-modulation doping, and an essentially large damping rate, the commercialization of on-chip QD lasers without optical isolation for data transmission on a PIC is within reach.

NARROW LINEWIDTH

Semiconductor lasers with narrow linewidths are of central interest in photonic applications where low phase noise is a prerequisite. The connection between the laser linewidth and the α -factor can be mathematically expressed as:

$$\Delta\nu = \frac{(\Gamma g_{\text{th}} v_g)^2 \eta_0}{4\pi P_0} h\nu n_{\text{sp}} (1 + \alpha^2), \quad (3)$$

where Γg_{th} is the threshold modal gain, v_g is the group velocity, $h\nu$ is the photon energy, n_{sp} is the population inversion factor, and η_0 and P_0 are the single facet optical efficiency and output power, respectively.

With an α -factor in the range of 2–6, traditional QW DFB or distributed Bragg reflection (DBR) lasers typically have linewidths on the order of a few megahertz. To reduce the laser linewidth to the kilohertz regime and ultimately reach into the sub kilohertz range, various efforts have been conducted, including external cavity designs [104]–[106] and heterogeneous Si/indium phosphide (InP) photonic platforms [107], [108]. However, these devices either remain significantly bulky or require much more process complexity as opposed to the standard DFB/DBR lasers.

Recently, a large linewidth reduction has been achieved in DFB lasers when the inherent properties of the optical active material are used, i.e., replacing the QWs with QDs. From the scaling relations, a reduction in the absolute value of the α -factor can induce large reductions in the laser linewidth by a factor of $(1 + \alpha^2)$. For a 1.55- μm QD DFB laser having an α -factor of 0.5, the reduction of the α -factor from 4 to 0.5 results in a 13 times reduction in linewidth. This translates into measured linewidths as narrow as 60 kHz (30 \pm 10 kHz intrinsic linewidth), which is more than one order of magnitude lower than those obtained in comparable QW DFB lasers [109].

Following this demonstration, a parametric model was developed. Based on this model, state-of-the-art 1,550-nm InAs/InP QD DFB lasers can achieve linewidths of less than 50 kHz at 20 °C and only slightly broaden to less than 80 kHz at 80 °C [110]. In the 1.3- μm region, QD DFBs achieve a linewidth–power product of 1.2 MHz mW, which is more than one order of magnitude lower than the typical value in QW DFBs [111]. Using a simple, integrable architecture without involving regrowth steps or subwavelength grating lithography, a tunable

single-wavelength QD laser directly grown on Si (Figure 7) achieved a 469-kHz Lorentzian linewidth with greater than 45-dB SMSR [112].

In this design, two all-active ring resonators (R_1 , R_2) with slightly different radii are cascaded to shape the Vernier spectrum needed for wavelength tuning. The two ring resonators are coupled to a common FP cavity by two half-wave couplers, which are designed to maintain low cross-coupling coefficients with a 180° phase difference for high single-mode selectivity [113]. A SEM image of the fabricated device and the schematic illustration are presented in the inset in Figure 7(a) and (c), respectively.

The resonant frequency combs of the three cavities and the material gain spectrum are schematically illustrated in Figure 7(b) to demonstrate the tuning principle. Using a commercial phase noise measurement system, a white noise floor of SF(f) = 1.5 \times 10⁵ Hz²/Hz level was measured, corresponding to a Lorentzian linewidth of 469 kHz [Figure 7(a)]. Lasing spectra across the tuning range can be measured by pumping the half-wave coupler and FP cavity region to transparency and tuning the current in either ring resonator. By changing the injection current on R_1 while keeping the other three electrodes biased at fixed current values as $I_c = 67$ mA, $I_{\text{FP}} = 79$ mA, and $I_{r2} = 30$ mA, respectively, 11-channel and 37-channel wavelength switching can be achieved, with minimum SMSR of 45 dB [Figure 7(c)] and 30 dB [112], respectively. In addition, a similar structure grown on a GaAs substrate achieved 716-kHz Lorentzian linewidth, 4-GHz 3-dB bandwidth, and 8-Gb/s nonreturn to zero (NRZ) signal modulation by directly probing the chip [114].

BETTER MODE LOCKING

Semiconductor mode-locked lasers (MLLs) possess the capability to generate ultrashort pulse trains as well as coherent optical frequency combs. This makes them promising compact light sources for short-distance wavelength-division multiplexing (WDM), photonic assisted analog-to-digital conversion, and on-chip clock recovery applications for

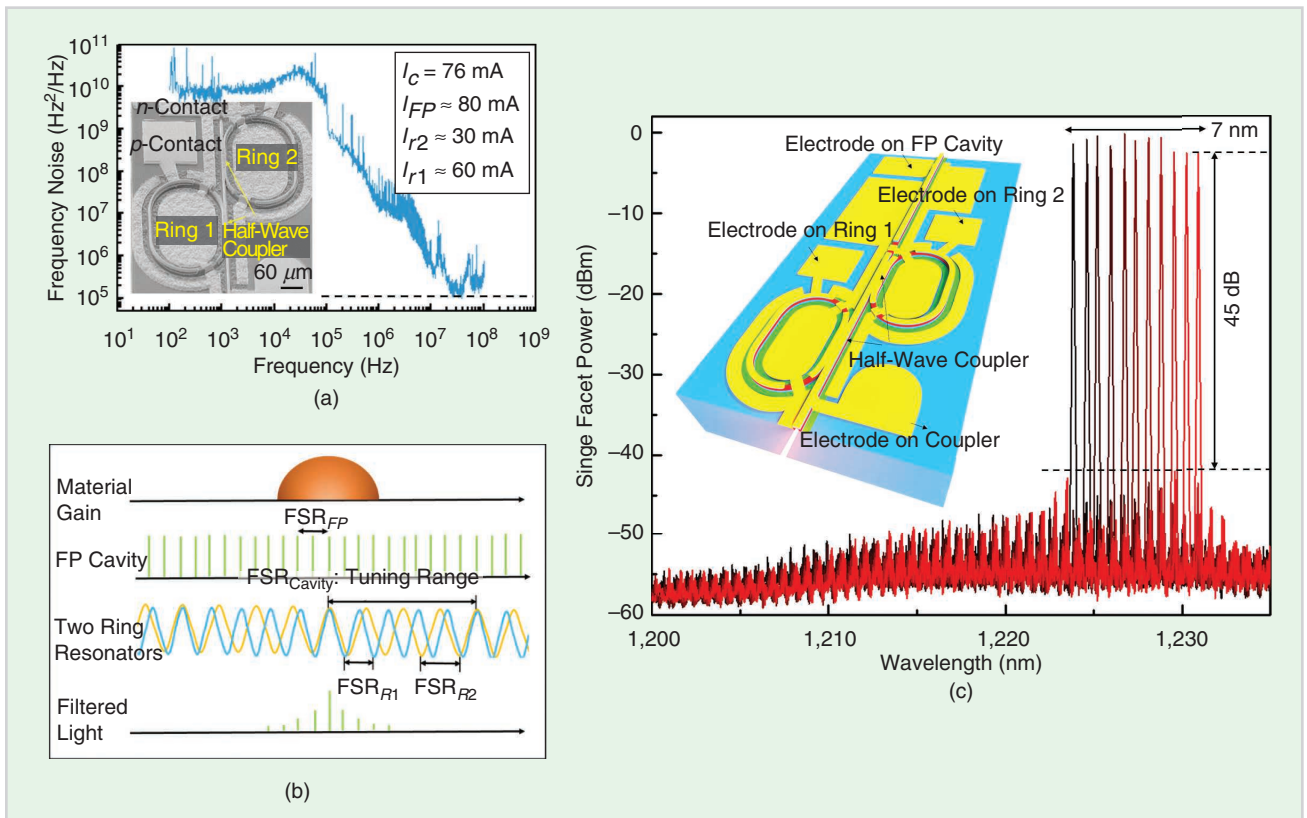


FIGURE 7 An Si-based tunable QD laser. (a) The frequency noise spectrum. Inset: a cross-sectional SEM of the laser architecture. (b) A schematic diagram illustrating the tuning principle of the tunable laser comprising two all-active ring resonators coupled to a common FP cavity. (c) The superimposed tuning spectra with 11-channel wavelength switching and a minimum SMSR of 45 dB. Inset: a schematic image of the tunable laser structure. FSR: free spectral range.

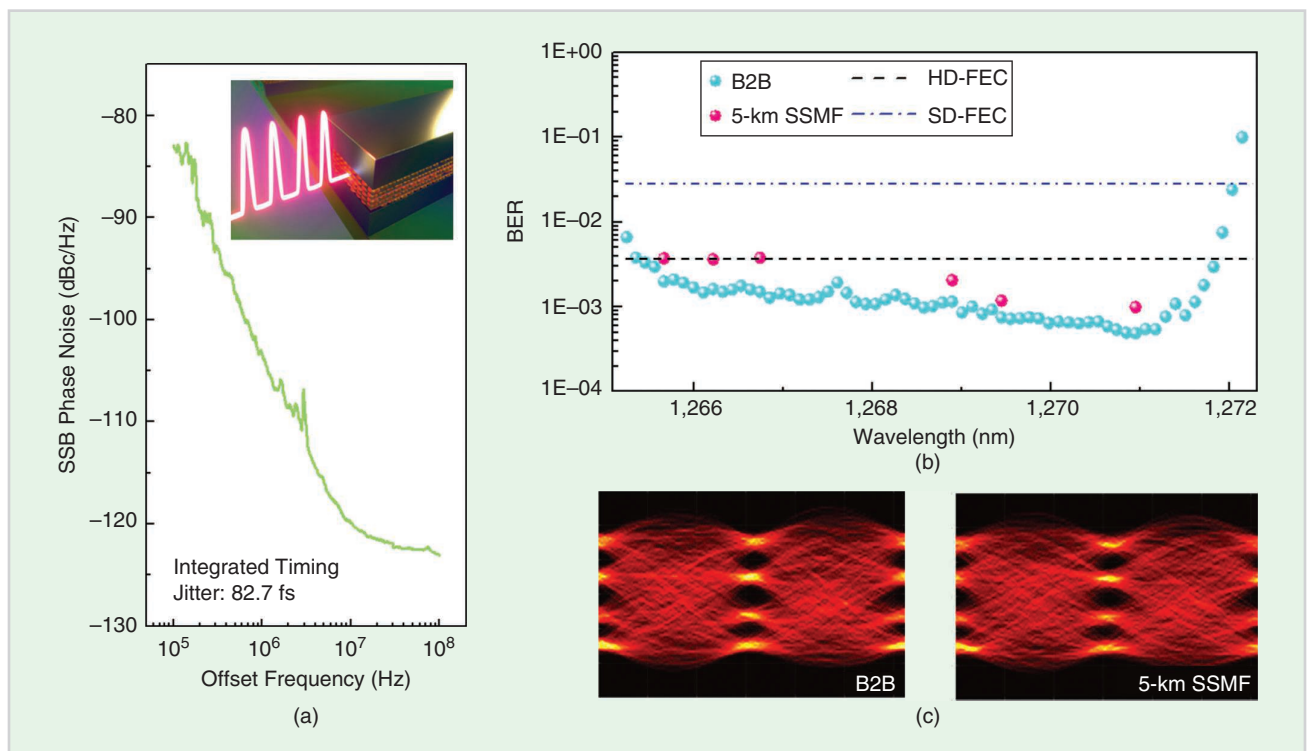


FIGURE 8 Si-based passively mode-locked 20-GHz QD MLL. (a) A single-sideband (SSB) phase noise plot under the narrowest pulsewidth condition ($I_{\text{gain}} = 110 \text{ mA}$, $V_{\text{SA}} = -5 \text{ V}$), showing an integrated timing jitter of 286 fs from 100 kHz to 100 MHz and 82.7 fs from 4 to 80 MHz. Inset: a schematic of the MLL. (b) The BER performance of the four-level pulse amplitude modulation (PAM-4) signal with different comb lines. (c) The corresponding eye diagrams for channels at 1,269.445 nm after B2B and 5-km SSMF transmission [122]. SD-FEC: soft-decision forward error correction.

which high repetition rate pulse sources with low amplitude noise, low timing jitter, high peak power, and narrow RF linewidths are of utmost importance

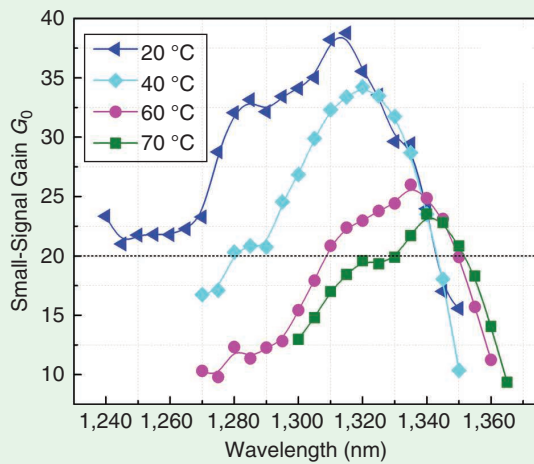
[115]. Ever since the first demonstration with a bulk active material system [116], pronounced improvements in mode-locking performance have been achieved

by modifying the DOS function to a 1D confinement of the carriers in a QW active region and, in the ultimate case, to a 3D confinement of the carriers in a QD active region. The higher dimensional confinement of carriers gives rise to an increased ratio of saturation energies in the gain and absorber sections, which is a key mode-locking parameter [117].

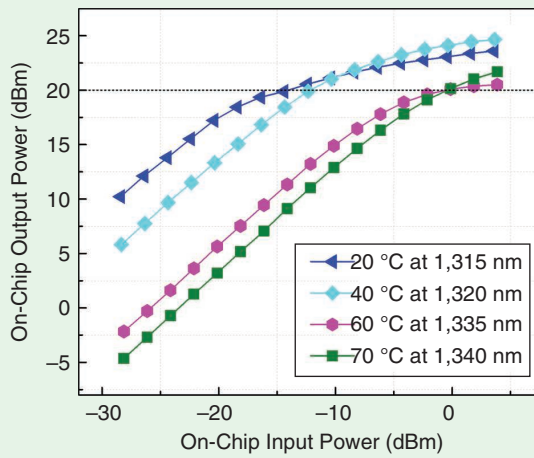
In addition to the delta-like DOS function in QDs, the broad gain spectrum predicts a theoretical minimum pulsewidth below 100 fs [118]. The small α -factor is beneficial for low-chirp, Fourier-limited pulses [14]. The low threshold current densities, internal loss, and confinement factor help to reduce noise [119]. The ultrafast gain/absorption recovery stages and low saturation energies contribute to a stable, wide range and low jitter mode locking [120], and the suppressed lateral carrier diffusion gives rise to low beam filamentation and negligible sidewall carrier recombination for deep mesa devices [121]. All of these combined parameters profoundly improved the mode-locking performance in terms of stability, pulse duration, chirp, output power, and noise.

A benchmark of the performance of monolithic multisection passively mode-locked QD lasers has been summarized in [123]. In many aspects, QD mode-locked lasers outperformed their QW counterparts [124]. For monolithic passively mode-locked QD lasers grown on native substrates, an ultrashort optical pulse of 360 fs [117] and a record-low 500-Hz RF linewidth [125] have been reported. Sixteen quadrature amplitude modulation dual-polarization WDM transmission on 38 channels at an aggregate net data rate of 10.68 Tb/s over 75 km of standard single-mode fiber have been achieved without any hardware-based phase noise reduction schemes [126].

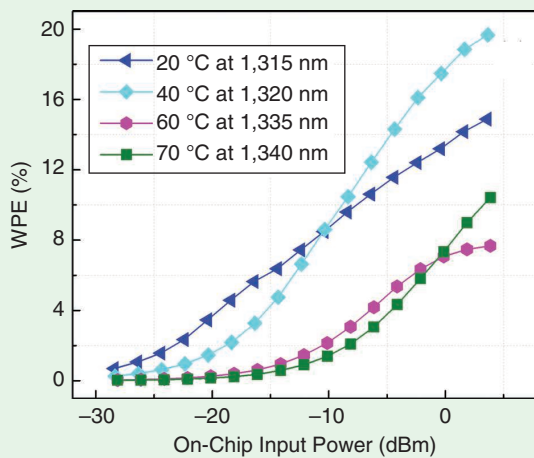
For passively mode-locked QD lasers directly grown on Si substrates, the lowest timing jitter value of 82.7 fs at a repetition rate of 20 GHz has been demonstrated [Figure 8(a)]. Sixty-four channels with BERs below the soft-decision forward



(a)



(b)



(c)

FIGURE 9 An Si-based QD SOA performance comparison under different stage temperatures: (a) on-chip small signal gain as a function of wavelength, (b) on-chip output power at gain peak as a function of on-chip input power, and (c) WPE at gain peak as a function of on-chip input power. ($I_{\text{gain}} = 750 \text{ mA}$, $T_{\text{stage}} = 20, 40, 60, \text{ and } 70 \text{ }^\circ\text{C}$, respectively.)

error correction (SD-FEC) threshold [Figure 8(b)] have been used in the back-to-back (B2B) and 5-km standard single-mode fiber (SSMF) transmission experiment. With a 32-GBaud Nyquist PAM-4 format, clear eye openings have been observed for both the B2B and the 5-km SSMF transmission and for the representative eye diagrams at 1,269.445 nm, as depicted in Figure 8(c). An aggregate total transmission capacity of 4.1 Tb/s is realized, demonstrating Tb-capable WDM interconnect networks.

SEMICONDUCTOR OPTICAL AMPLIFIERS

High gain and saturation output power SOAs are important building blocks in future large-scale PICs to allow for scaling to thousands of optical elements and to compensate for the losses introduced by large numbers of passive and active components [127]. In-line SOAs are a natural solution to address the accumulated insertion loss issues from those passive switches, waveguide crossings, and couplers, which would help alleviate the requirement on the light source side as well as compensate for the path loss to maintain channel equalization.

Recent reports of the SOAs on Si generally leverage flip chip bonding or wafer bonding technologies of QW gain regions, with excellent performance in the C-band demonstrated [128], [129]. Greater than 26-dB on-chip gain [130], 17-dBm saturation output power [131], and 12.1% wall-plug efficiency (WPE) [132] have been demonstrated. O-band Si PICs are a hot topic recently, driven by the huge traffic in data centers and passive optical networks [133], and the developed InAs QD direct growth platform for lasers can be used naturally to realize on-chip O-band SOAs.

QD gain media for SOAs has multiple advantages compared to its counterparts. The fast gain response makes it suitable to amplify high-speed signals without pattern effects; the high temperature stability leads to uncooled operation; the low threshold current density, internal loss, and confinement factor contribute to low noise figure operation; and the inhomogeneously broadened gain translates to

a wide amplification bandwidth [29], [83], [134]. The first QD SOA directly grown on Si with high gain and large amplification bandwidth has recently been reported [28]. It leverages a tapered gain section design to enlarge the mode area for enhancing the saturation output power. The QD region spacer layer was p-modulation doped to improve the temperature stability. The device demonstrates a maximum on-chip gain of 39 dB, minimum noise figure of 6.6 dB, saturation output power of 24 dBm, > 100-nm amplification bandwidth (i.e., gain > 20 dB), and a WPE of 20% (Figure 9). The introduction of p-modulation doping effectively extends the device operation to 70 °C with > 20 dB gain in a 21-nm wavelength range.

The improvement in receiver sensitivity by using QD optical preamplification is illustrated in Figure 10 in a filterless 60-Gb/s NRZ transmission system [28]. A 15-dB photodiode sensitivity improvement (−25 dBm minimum sensitivity) can be obtained at 20 °C. Minimum receiver sensitivities of −20 and −13 dBm can be obtained under elevated stage temperatures at 40 and 60 °C, respectively, at the KR4-FEC coding limit. The effective sensitivity enhancement bandwidths are

60, 30, and 10 nm, respectively, for the temperatures of 20, 40, and 60 °C.

CONCLUSION

In summary, recent advances in the physics and applications of 1.3- μm self-assembled QD lasers have been reviewed, concentrating on six key areas, namely, the large tolerance to material defects that allows for the epitaxial integration of QD lasers on Si, the much-reduced reflection sensitivity feedback that offers the prospect of eliminating optical isolators in PICs, the low α -factors resulting in narrow linewidth lasers, the ultrafast gain dynamics useful for semiconductor mode-locked lasers, and the record-low threshold currents and high temperature stability of these lasers.

Significant improvements in III-V/Si epitaxy have pushed QD technology to the frontiers of Si photonics and to a wide range of applications. Still, much effort is needed to make this technology ubiquitous and affordable for high-volume, high-performance PICs. To name a few, a systematic study of reliability and reproducibility with high power testing is needed to prove laser viability at data center ambient temperatures, and wafer scale growth and yield on 300-mm Si substrates are required to demonstrate

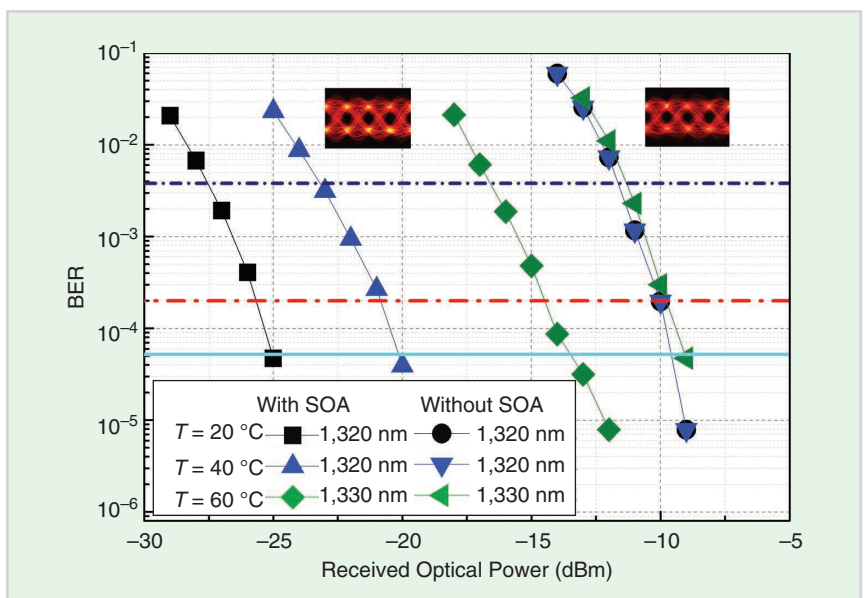


FIGURE 10 The BER against the received optical power for the optical receiver (PD+TIA) with and without QD SOA under a range of temperatures including 20, 40, and 60 °C. Eye diagrams of the receiver with and without QD SOA are shown in the insets [28]. PD: photodiode; TIA: transimpedance amplifier.

the economies of scale in photonic integration via epitaxial III-V on Si.

In terms of integration via epitaxy, the majority of research still focuses on individual devices, particularly lasers. The performance of amplifiers, photodetectors, and modulators using QD materials needs to be demonstrated. Low-loss active-passive coupling schemes need to be developed to integrate these QD-based components with waveguides, preferably in Si photonics. The key next step will be demonstrating a platform that allows for epitaxial integration to best leverage the economies of scale of Si while maintaining the highest yield at the lowest lifecycle cost.

ACKNOWLEDGMENTS

The University of California Santa Barbara work was funded by DARPA Microsystems Technology Office and by the Advanced Research Projects Agency-Energy, U.S. Department of Energy, under award DE-AR0001042 and DE-AR0001039. The authors are grateful to Art Gossard, Frederic Grillot, Weng W. Chow, Kunal Mukherjee, Chen Shang, Dachwan Jung, Di Liang, Chong Zhang, Chao Xiang, Minh Tran, Duanni Huang, and M.J. Kennedy for their helpful suggestions and discussions. The views and opinions of the authors expressed herein do not necessarily state or reflect those of the U.S. Government or any agency thereof.

ABOUT THE AUTHORS

Yating Wan (yatingwan@ucsb.edu) is with the Institute for Energy Efficiency, University of California, Santa Barbara, Santa Barbara, California, 93106, USA.

Justin Norman (jcnorman223@gmail.com) is with the Materials Department, University of California, Santa Barbara, Santa Barbara, California, 93106, USA.

Songtao Liu (songtao_liu@ucsb.edu) is with the Department of Electrical and Computer Engineering, University of California, Santa Barbara, Santa Barbara, California, 93106, USA.

Alan Liu (alan@quintessent.com) is with Quintessent, Inc., Santa Barbara, California, 93102, USA.

John E. Bowers (bowers@ece.ucsb.edu) is with the Institute for Energy Efficiency, the Materials Department,

and the Department of Electrical and Computer Engineering, University of California, Santa Barbara, Santa Barbara, California, 93106, USA.

REFERENCES

- [1] Y. Arakawa and H. Sakaki, "Multidimensional quantum well laser and temperature dependence of its threshold current," *Appl. Phys. Lett.*, vol. 40, no. 11, pp. 939–941, 1982. doi: 10.1063/1.92959.
- [2] N. N. Ledentsov, V. M. Ustinov, V. A. Shchukin, P. S. Kop'Ev, Z. I. Alferov, and D. Bimberg, "Quantum dot heterostructures: Fabrication, properties, lasers," *Semiconductors*, vol. 32, no. 4, pp. 343–365, 1998. doi: 10.1134/1.1187396.
- [3] L. V. Asryan and R. A. Suris, "Theory of threshold characteristics of semiconductor quantum dot lasers," *Semiconductors*, vol. 38, no. 1, pp. 1–22, Jan. 2004. doi: 10.1134/1.1641126.
- [4] A. E. Zhukov, M. V. Maksimov, and A. R. Kovsh, "Device characteristics of long-wavelength lasers based on self-organized quantum dots," *Semiconductors*, vol. 46, no. 10, pp. 1225–1250, 2012. doi: 10.1134/S1063782612100223.
- [5] L. Goldstein, F. Glas, J. Y. Marzin, M. N. Charasse, and G. Le Roux, "Growth by molecular beam epitaxy and characterization of InAs/GaAs strained-layer superlattices," *Appl. Phys. Lett.*, vol. 47, no. 10, pp. 1099–1101, 1985. doi: 10.1063/1.96342.
- [6] R. P. Mirin, J. P. Ibbetson, K. Nishi, A. C. Gossard, and J. E. Bowers, "1.3 μm photoluminescence from InGaAs quantum dots on GaAs," *Appl. Phys. Lett.*, vol. 67, no. 25, pp. 3795–3797, 1995. doi: 10.1063/1.115386.
- [7] R. Mirin, A. Gossard, and J. Bowers, "Room temperature lasing from InGaAs quantum dots," *Electron. Lett.*, vol. 32, no. 18, p. 1732, 1996. doi: 10.1049/el:19961147.
- [8] T. Ishikawa, S. Kohmoto, and K. Asakawa, "Site control of self-organized InAs dots on GaAs substrates by in situ electron-beam lithography and molecular-beam epitaxy," *Appl. Phys. Lett.*, vol. 73, no. 12, pp. 1712–1714, 1998. doi: 10.1063/1.122254.
- [9] M. Lachab et al., "Selective fabrication of InGaN nanostructures by the focused ion beam/metalorganic chemical vapor deposition process," *J. Appl. Phys.*, vol. 87, no. 3, pp. 1374–1378, 2000. doi: 10.1063/1.372023.
- [10] T. Umeda, K. Kumakura, J. Motohisa, and T. Fukui, "InAs quantum dot formation on GaAs pyramids by selective area MOVPE," *Phys. E Low-Dimensional Syst. Nanostruct.*, vol. 2, nos. 1–4, pp. 714–719, July 1998. doi: 10.1016/S1386-9477(98)00146-5.
- [11] N. Kirstaedter et al., "Low threshold, large Toinjection laser emission from (InGa)As quantum dots," *Electron. Lett.*, vol. 30, no. 17, pp. 1416–1417, Aug. 1994. doi: 10.1049/el:19940939.
- [12] D. G. Deppe, K. Shavritanuruk, G. Ozgur, H. Chen, and S. Freisem, "Quantum dot laser diode with low threshold and low internal loss," *Electron. Lett.*, vol. 45, no. 1, pp. 54–56, 2009. doi: 10.1049/el:20092873.
- [13] J. Wu, S. Chen, A. Seeds, and H. Liu, "Quantum dot optoelectronic devices lasers, photodetectors and solar cells," *J. Phys. D. Appl. Phys.*, vol. 48, no. 36, p. 363,001, 2015. doi: 10.1088/0022-3727/48/36/363001.
- [14] D. Bimberg and U. W. Pohl, "Quantum dots: Promises and accomplishments," *Mater. Today*, vol. 14, no. 9, pp. 388–397, 2011. doi: 10.1016/S1369-7021(11)70183-3.
- [15] S. Fathpour et al., "The role of Auger recombination in the temperature-dependent out-

- put characteristics ($T_0=\infty$) of p -doped 1.3 μm quantum dot lasers," *Appl. Phys. Lett.*, vol. 85, no. 22, pp. 5164–5166, 2004. doi: 10.1063/1.1829158.
- [16] T. Kagayama et al., "Extremely high temperature (220°C) continuous-wave operation of 1300-nm-range quantum-dot lasers," in *Proc. Eur. Conf. Lasers Electro-Optics*, 2011, p. PDA_1.
- [17] Y. Urino et al., "First demonstration of athermal silicon optical interposers with quantum dot lasers operating up to 125°C," *J. Light. Technol.*, vol. 33, no. 6, pp. 1223–1229, 2015. doi: 10.1109/JLT.2014.2380811.
- [18] P. K. Kondratko, S. L. Chuang, G. Walter, T. Chung, and N. Holonyak, "Observations of near-zero linewidth enhancement factor in a quantum-well coupled quantum-dot laser," *Appl. Phys. Lett.*, vol. 83, no. 23, pp. 4818–4820, Dec. 2003. doi: 10.1063/1.1631397.
- [19] P. Bhattacharya and Z. Mi, "Quantum-dot optoelectronic devices," *Proc. IEEE*, vol. 95, no. 9, pp. 1723–1740, Sept. 2007. doi: 10.1109/JPROC.2007.900897.
- [20] Y. Wan et al., "Monolithically integrated InAs/InGaAs quantum dot photodetectors on silicon substrates," *Opt. Express*, vol. 25, no. 22, p. 27715, Oct. 2017. doi: 10.1364/OE.25.027715.
- [21] B. Tossoun et al., "Indium arsenide quantum dot waveguide photodiodes heterogeneously integrated on silicon," *Optica*, vol. 6, no. 10, p. 1277, Oct. 2019. doi: 10.1364/OPTICA.6.001277.
- [22] B. Chen et al., "Low dark current high gain InAs quantum dot avalanche photodiodes monolithically grown on Si," *ACS Photon.*, vol. 7, no. 2, pp. 528–533, Jan. 2020. doi: 10.1021/acsp Photonics.9b01709.
- [23] J. W. Kim, J. E. Oh, S. C. Hong, C. H. Park, and T. K. Yoo, "Room temperature far infrared (8–10 μm) photodetectors using self-assembled InAs quantum dots with high detectivity," *IEEE Electron Device Lett.*, vol. 21, no. 7, pp. 329–331, July 2000.
- [24] "FCI-InGaAs-36C 10Gbps InGaAs photodiode," OSI Optoelectronics Ltd., USA. Accessed: June 21, 2020. [Online]. Available: <http://www.osioptoelectronics.com/Libraries/Datasheets/FCI-InGaAs-36C.sflb.ashx>
- [25] J. Michel, J. Liu, and L. C. Kimerling, "High-performance Ge-on-Si photodetectors," *Nat. Photon.*, vol. 4, no. 8, pp. 527–534, Aug. 2010. doi: 10.1038/nphoton.2010.157.
- [26] J. Huang et al., "Defect characterization of InAs/InGaAs quantum dot p-i-n photodetector grown on GaAs-on-V-grooved-Si substrate," *ACS Photon.*, vol. 6, no. 5, pp. 1100–1105, May 2019. doi: 10.1021/acsp Photonics.8b01707.
- [27] Y. Wan et al., "Low-dark current 1.55 μm InAs quantum dash waveguide photodiodes," *ACS Nano*, vol. 14, no. 3, pp. 3519–3527, 2020. doi: 10.1021/acsnano.9b09715.
- [28] S. Liu et al., "High-performance O-band quantum-dot semiconductor optical amplifiers directly grown on a CMOS compatible silicon substrate," *ACS Photon.*, vol. 6, no. 10, pp. 2523–2529, 2019. doi: 10.1021/acsp Photonics.9b00903.
- [29] T. Akiyama, M. Sugawara, and Y. Arakawa, "Quantum-Dot Semiconductor Optical Amplifiers," *Proc. IEEE*, vol. 95, no. 9, pp. 1757–1766, 2007. doi: 10.1109/JPROC.2007.900899.
- [30] C. Meuer et al., "High-speed small-signal cross-gain modulation in quantum-dot semiconductor optical amplifiers at 1.3 μm ," *IEEE J. Sel. Top. Quantum Electron.*, vol. 15, no. 3, pp. 749–756, 2009. doi: 10.1109/JSTQE.2009.2012395.
- [31] V. Aroutiounian, S. Petrosyan, A. Khachatryan, and K. Touryan, "Quantum dot solar cells," *J. Appl. Phys.*, vol. 89, no. 4, pp. 2268–2271, 2001. doi: 10.1063/1.1339210.
- [32] C. G. Bailey et al., "Open-circuit voltage improvement of InAs/GaAs quantum-dot solar

- cells using reduced InAs coverage," *IEEE J. Photovoltaics*, vol. 2, no. 3, pp. 269–275, 2012. doi: 10.1109/JPHOTOV.2012.2189047.
- [33] Z. Mi, J. Yang, P. Bhattacharya, G. Qin, and Z. Ma, "High-performance quantum dot lasers and integrated optoelectronics on Si," *Proc. IEEE*, vol. 97, no. 7, pp. 1239–1249, July 2009. doi: 10.1109/JPROC.2009.2014780.
- [34] A. Y. Liu, S. Srinivasan, J. Norman, A. C. Gosard, and J. E. Bowers, "Quantum dot lasers for silicon photonics [Invited]," *Photon. Res.*, vol. 3, no. 5, p. B1, Oct. 2015. doi: 10.1364/PRJ.3.0000B1.
- [35] J. C. Norman, D. Jung, Y. Wan, and J. E. Bowers, "Perspective: The future of quantum dot photonic integrated circuits," *APL Photon.*, vol. 3, no. 3, p. 30,901, 2018. doi: 10.1063/1.5021345.
- [36] D. Jung et al., "A review of high performance quantum dot lasers on silicon," *IEEE J. Quantum Electron.*, vol. 55, no. 2, pp. 1–11, 2019. doi: 10.1109/JQE.2019.2901508.
- [37] Q. Feng et al., "O-Band and C-L-Band III-V quantum dot lasers monolithically grown on Ge and Si substrate," *Appl. Sci.*, vol. 9, no. 3, p. 385, Jan. 2019. doi: 10.3390/app9030385.
- [38] N. V. Kryzhanovskaya, M. V. Maximov, and A. E. Zhukov, "Whispering-gallery mode microcavity quantum-dot lasers," *Quantum Electron.*, vol. 44, no. 3, p. 189, 2014. doi: 10.1070/QE2014v04n03ABEH015358.
- [39] Y. Wan, J. Norman, and J. Bowers, "Quantum dot microcavity lasers," in *Semiconductors and Semimetals*, New York: Elsevier, 2019, vol. 101, pp. 305–354.
- [40] Y. Wan et al., "O-band electrically injected quantum dot micro-ring lasers on on-axis (001) GaP/Si and V-groove Si," *Opt. Express*, vol. 25, no. 22, pp. 26,853–26,860, Oct. 2017. doi: 10.1364/OE.25.026853.
- [41] S. Pan et al., "Recent progress in epitaxial growth of III-V quantum-dot lasers on silicon substrate," *J. Semicond.*, vol. 40, no. 10, p. 101,302, 2019. doi: 10.1088/1674-4926/40/10/101302.
- [42] D. Bimberg et al., "Quantum dot lasers: Breakthrough in optoelectronics," *Thin Solid Films*, vol. 367, nos. 1–2, pp. 235–249, 2000. doi: 10.1016/S0040-6090(00)00697-0.
- [43] N. Chand, E. E. Becker, J. P. Van Der Ziel, S. N. G. Chu, and N. K. Dutta, "Excellent uniformity and very low (<50 A/cm²) threshold current density strained InGaAs quantum well diode lasers on GaAs substrate," *Appl. Phys. Lett.*, vol. 58, no. 16, pp. 1704–1706, 1991.
- [44] Y. Wan et al., "Low threshold quantum dot lasers directly grown on planar (001) Si," *IEEE J. Sel. Top. Quantum Electron.*, vol. 26, no. 2, pp. 1–9, 2020. doi: 10.1109/JSTQE.2020.2964381.
- [45] S. Chen et al., "Electrically pumped continuous-wave III-V quantum dot lasers on silicon," *Nat. Photon.*, vol. 10, no. 5, pp. 307–311, May 2016. doi: 10.1038/nphoton.2016.21.
- [46] D. Jung et al., "High efficiency low threshold current 1.3 μm InAs quantum dot lasers on on-axis (001) GaP/Si," *Appl. Phys. Lett.*, vol. 111, no. 12, p. 122,107, 2017. doi: 10.1063/1.4993226.
- [47] Y. Wan et al., "1.3 μm submilliampere threshold quantum dot micro-lasers on Si," *Optica*, vol. 4, no. 8, pp. 940–944, 2017. doi: 10.1364/OPTICA.4.000940.
- [48] Y. Wan et al., "Optically pumped 1.3 μm room-temperature InAs quantum-dot micro-disk lasers directly grown on (001) silicon," *Opt. Lett.*, vol. 41, no. 7, pp. 1664–1667, 2016. doi: 10.1364/OL.41.001664.
- [49] Y. Wan et al., "Directly modulated quantum dot lasers on silicon with a milliampere threshold and high temperature stability," *Photon. Res.*, vol. 6, no. 8, p. 776, Aug. 2018. doi: 10.1364/PRJ.6.000776.
- [50] Y. Wan et al., "Low-threshold continuous-wave operation of electrically pumped 1.55 μm InAs quantum dash microring lasers," *ACS Photon.*, vol. 6, no. 2, pp. 279–285, Feb. 2019. doi: 10.1021/acsphotonics.8b01341.
- [51] T. Zhou et al., "Continuous-wave quantum dot photonic crystal lasers grown on on-axis Si (001)," *Nat. Commun.*, vol. 11, no. 1, pp. 1–7, Dec. 2020.
- [52] Y. Wan et al., "Temperature characteristics of epitaxially grown InAs quantum dot micro-disk lasers on silicon for on-chip light sources," *Appl. Phys. Lett.*, vol. 109, no. 1, p. 011104, July 2016. doi: 10.1063/1.4955456.
- [53] Q. Li et al., "1.3 μm InAs quantum-dot micro-disk lasers on V-groove patterned and unpatterned (001) silicon," *Opt. Express*, vol. 24, no. 18, pp. 21,038–21,045, Sept. 2016. doi: 10.1364/OE.24.021038.
- [54] S. A. Moore, L. O'Faolain, M. A. Cataluna, M. B. Flynn, M. V. Kotlyar, and T. F. Krauss, "Reduced surface sidewall recombination and diffusion in quantum-dot lasers," *IEEE Photon. Technol. Lett.*, vol. 18, no. 17, pp. 1861–1863, 2006. doi: 10.1109/LPT.2006.881206.
- [55] S. Strauf et al., "Self-tuned quantum dot gain in photonic crystal lasers," *Phys. Rev. Lett.*, vol. 96, no. 12, p. 127,404, 2006.
- [56] Y. Wan et al., "Sub-wavelength InAs quantum dot micro-disk lasers epitaxially grown on exact Si (001) substrates," *Appl. Phys. Lett.*, vol. 108, no. 22, p. 221,101, 2016. doi: 10.1063/1.4952600.
- [57] Y. Wan et al., "Quadruple reduction of threshold current density for micro-ring quantum dot lasers epitaxially grown on (001) Si," in *Proc. Conf. Lasers Electro-Optics*, 2018, p. SW3Q.3.
- [58] O. B. Shechkin and D. G. Deppe, "The role of p-type doping and the density of states on the modulation response of quantum dot lasers," *Appl. Phys. Lett.*, vol. 80, no. 15, pp. 2758–2760, 2002. doi: 10.1063/1.1469212.
- [59] QD Laser Inc. Accessed: June 21, 2020. [Online]. Available: <https://www.qdlaser.com/en/products/list.html>
- [60] A. Liu et al., "High performance continuous wave 1.3 μm quantum dot lasers on silicon," *Appl. Phys. Lett.*, vol. 104, no. 4, p. 41,104, 2014.
- [61] J. C. Norman et al., "The importance of p-doping for quantum dot laser on silicon performance," *IEEE J. Quantum Electron.*, vol. 55, no. 6, pp. 1–11, 2019. doi: 10.1109/JQE.2019.2941579.
- [62] Y. Wan et al., "Sub-mA threshold 1.3 μm CW lasing from electrically pumped microrings grown on (001) Si," in *Proc. Conf. Lasers Electro-Optics (CLEO)*, 2017, pp. 1–2.
- [63] T. H. Windhorn, G. M. Metzger, B. Y. Tsaui, and J. C. C. Fan, "AlGaAs double-heterostructure diode lasers fabricated on a monolithic GaAs/Si substrate," *Appl. Phys. Lett.*, vol. 45, no. 4, pp. 309–311, 1984. doi: 10.1063/1.95273.
- [64] H. Z. Chen, A. Ghaffari, H. Wang, H. Morkoç, and A. Yariv, "Continuous-wave operation of extremely low-threshold GaAs/AlGaAs broad-area injection lasers on (100) Si substrates at room temperature," *Opt. Lett.*, vol. 12, no. 10, p. 812, 1987. doi: 10.1364/OL.12.000812.
- [65] R. D. Dupuis, J. P. Van Der Ziel, R. A. Logan, J. M. Brown, and C. J. Pinzone, "Low-threshold high-efficiency AlGaAs–GaAs double-heterostructure injection lasers grown on Si substrates by metalorganic chemical vapor deposition," *Appl. Phys. Lett.*, vol. 50, no. 7, pp. 407–409, 1987. doi: 10.1063/1.98185.
- [66] H. Z. Chen, J. Paslaski, A. Ghaffari, H. Wang, H. Morkoç, and A. Yariv, "High speed modulation and CW operation of AlGaAs/GaAs lasers on Si," in *Proc. Tech. Dig. – Int. Electron Devices Meeting*, 1987, pp. 238–241.
- [67] J. P. Van Der Ziel, R. D. Dupuis, R. A. Logan, and C. J. Pinzone, "Degradation of GaAs lasers grown by metalorganic chemical vapor deposition on Si substrates," *Appl. Phys. Lett.*, vol. 51, no. 2, pp. 89–91, 1987. doi: 10.1063/1.98997.
- [68] M. E. Groenert, A. J. Pitera, R. J. Ram, and E. A. Fitzgerald, "Improved room-temperature continuous wave GaAs/AlGaAs and InGaAs/GaAs/AlGaAs lasers fabricated on Si substrates via relaxed graded GeSi_{1-x} buffer layers," *J. Vac. Sci. Technol. B Microelectron. Nanom. Struct.*, vol. 21, no. 3, pp. 1064–1069, 2003. doi: 10.1116/1.1576397.
- [69] S. F. Fang et al., "Gallium arsenide and other compound semiconductors on silicon," *J. Appl. Phys.*, vol. 68, no. 7, pp. R31–R58, 1990. doi: 10.1063/1.346284.
- [70] B. Kunert, Y. Mols, M. Baryshnikova, N. Waldron, A. Schulze, and R. Langer, "How to control defect formation in monolithic III/V hetero-epitaxy on (100) Si? A critical review on current approaches," *Semicond. Sci. Technol.*, vol. 33, no. 9, p. 93,002, 2018.
- [71] Y. B. Bolkhovityanov and O. P. Pchelyakov, "GaAs epitaxy on Si substrates: Modern status of research and engineering," *Phys. Uspekhi*, vol. 51, no. 5, p. 437, 2008. doi: 10.1070/PU2008v051n05ABEH006529.
- [72] Q. Li and K. M. Lau, "Epitaxial growth of highly mismatched III-V materials on (001) silicon for electronics and optoelectronics," *Prog. Cryst. Growth Charact. Mater.*, vol. 63, no. 4, pp. 105–120, 2017. doi: 10.1016/j.pcrysgrow.2017.10.001.
- [73] O. Supplie et al., "Metalorganic vapor phase epitaxy of III-V-on-silicon: Experiment and theory," *Prog. Cryst. Growth Charact. Mater.*, vol. 64, no. 4, pp. 103–132, 2018. doi: 10.1016/j.pcrysgrow.2018.07.002.
- [74] C. Shang et al., "Low-threshold epitaxially grown 1.3-μm InAs quantum dot lasers on patterned (001) Si," *IEEE J. Sel. Top. Quantum Electron.*, vol. 25, no. 6, pp. 1–7, 2019. doi: 10.1109/JSTQE.2019.2927581.
- [75] C. Shang et al., "A pathway to thin GaAs virtual substrate on on-axis Si(001) with ultralow threading dislocation density," *Phys. Status Solidi*, p. 2000402, 2020. doi: 10.1002/psa.202000402.
- [76] Z. I. Kazi, P. Thilakan, T. Egawa, M. Umeno, and T. Jimbo, "Realization of GaAs/AlGaAs lasers on Si substrates using epitaxial lateral overgrowth by metalorganic chemical vapor deposition," *Jpn. J. Appl. Phys.*, vol. 40, no. 8R, pp. 4903–4906, 2001. doi: 10.1143/JJAP.40.4903.
- [77] K. K. Linder et al., "Self-organized In_{0.4}Ga_{0.6}As quantum-dot lasers grown on Si substrates," *Appl. Phys. Lett.*, vol. 74, no. 10, pp. 1355–1357, 1999. doi: 10.1063/1.123548.
- [78] A. Y. Liu, R. W. Herrick, O. Ueda, P. M. Petroff, A. C. Gosard, and J. E. Bowers, "Reliability of InAs/GaAs quantum dot lasers epitaxially grown on silicon," *IEEE J. Sel. Top. Quantum Electron.*, vol. 21, no. 6, pp. 690–697, 2015. doi: 10.1109/JSTQE.2015.2418226.
- [79] D. Jung et al., "Highly reliable low-threshold InAs quantum dot lasers on on-axis (001) Si with 87% injection efficiency," *ACS Photon.*, vol. 5, no. 3, pp. 1094–1100, 2017. doi: 10.1021/acsphotonics.7b01387.
- [80] O. Ueda and S. J. Pearton, Eds., *Materials and Reliability Handbook for Semiconductor Optical and Electron Devices*. New York: Springer Science & Business Media, 2013.
- [81] J. Selvidge et al., "Non-radiative recombination at dislocations in InAs quantum dots grown on silicon," *Appl. Phys. Lett.*, vol. 115, no. 13, p. 131,102, Sept. 2019. doi: 10.1063/1.5113517.
- [82] M. Buffolo et al., "Investigation of current-driven degradation of 1.3 μm quantum-dot lasers epitaxially grown on silicon," *IEEE J. Sel. Top. Quantum Electron.*, vol. 26, no. 2, 2020, Art. no. 1900208. doi: 10.1109/JSTQE.2019.2939519.
- [83] T. W. Berg and J. Mork, "Saturation and noise properties of quantum-dot optical amplifiers," *IEEE J. Quantum Electron.*, vol. 40,

- no. 11, pp. 1527–1539, 2004. doi: 10.1109/JQE.2004.835114.
- [84] C. Hantschmann et al., “Theoretical study on the effects of dislocations in monolithic III-V lasers on silicon,” *J. Light. Technol.*, vol. 38, no. 17, pp. 4801–4807, May 2020.
- [85] R. Leon et al., “Changes in luminescence emission induced by proton irradiation: InGaAs/GaAs quantum wells and quantum dots,” *Appl. Phys. Lett.*, vol. 76, no. 15, pp. 2074–2076, 2000. doi: 10.1063/1.126259.
- [86] C. Ribbat, R. Sellin, M. Grundmann, D. Bimberg, N. A. Sobolev, and M. C. Carmo, “Enhanced radiation hardness of quantum dot lasers to high energy proton irradiation,” *Electron. Lett.*, vol. 37, no. 3, p. 174, 2001. doi: 10.1049/el:20010118.
- [87] M. Buffolo et al., “Physical origin of the optical degradation of InAs quantum dot lasers,” *IEEE J. Quantum Electron.*, vol. 55, no. 3, pp. 1–7, 2019. doi: 10.1109/JQE.2019.2909963.
- [88] I. O’Driscoll, P. Blood, A. Sobiesierski, R. Gwilliam, and P. M. Smowton, “Evaluating InAs QD lasers for space borne applications,” in *Proc. Int. Semiconductor Laser Conf. (ISLC 2012)*, 2012, pp. 94–95.
- [89] D. Jung et al., “Impact of threading dislocation density on the lifetime of InAs quantum dot lasers on Si,” *Appl. Phys. Lett.*, vol. 112, no. 15, p. 153507, 2018. doi: 10.1063/1.5026147.
- [90] M. Osinski and J. Buus, “Linewidth broadening factor in semiconductor lasers – An overview,” *IEEE J. Quantum Electron.*, vol. 23, no. 1, pp. 9–29, 1987. doi: 10.1109/JQE.1987.1073204.
- [91] L. A. Coldren, S. W. Corzine, and M. L. Mashanovitch, *Diode Lasers and Photonic Integrated Circuits*. Hoboken, NJ: Wiley, 2012.
- [92] Z. Zhang, D. Jung, J. Norman, W. W. Chow, and J. E. Bowers, “Linewidth enhancement factor in InAs/GaAs quantum dot lasers and its implication in isolator-free and narrow linewidth applications,” *IEEE J. Sel. Top. Quantum Electron.*, vol. 25, no. 6, pp. 1–9, 2019. doi: 10.1109/JSTQE.2019.2916884.
- [93] D. Bimberg, N. Kirstaedter, N. N. Ledentsov, Z. I. Alferov, P. S. Kop’ev, and V. M. Ustinov, “InGaAs-GaAs quantum-dot lasers,” *IEEE J. Sel. Top. Quantum Electron.*, vol. 3, no. 2, pp. 196–205, 1997. doi: 10.1109/2944.605656.
- [94] J. Duan et al., “1.3- μm reflection insensitive InAs/GaAs quantum dot lasers directly grown on silicon,” *IEEE Photon. Technol. Lett.*, vol. 31, no. 5, pp. 345–348, 2019. doi: 10.1109/LPT.2019.2895049.
- [95] Z. Zhang, D. Jung, J. C. Norman, P. Patel, W. W. Chow, and J. E. Bowers, “Continuous tuning of gain peak linewidth enhancement factor from negative to positive with p doping in InAs QD laser on Si,” in *Proc. IEEE Int. Semicond. Laser Conf. (ISLC)*, 2018, pp. 1–2. doi: 10.1109/ISLC.2018.8516259.
- [96] D. Huang, P. Pintus, C. Zhang, Y. Shoji, T. Mizumoto, and J. E. Bowers, “Electrically driven and thermally tunable integrated optical isolators for silicon photonics,” *IEEE J. Sel. Top. Quantum Electron.*, vol. 22, no. 6, pp. 271–278, Nov. 2016. doi: 10.1109/JSTQE.2016.2588778.
- [97] D. O’Brien et al., “Feedback sensitivity of 1.3 μm InAs/GaAs quantum dot lasers,” *Electron. Lett.*, vol. 39, no. 25, pp. 1819–1820, 2003.
- [98] Y. Wan et al., “1.3 μm quantum dot-distributed feedback lasers directly grown on (001) Si,” *Laser Photon. Rev.*, vol. 14, no. 7, p. 2,000,037, June 2020. doi: 10.1002/lpor.202000037.
- [99] J. Wang and K. Petermann, “Noise analysis of semiconductor lasers within the coherence collapse regime,” *IEEE J. Quantum Electron.*, vol. 27, no. 1, pp. 3–9, 1991. doi: 10.1109/3.73534.
- [100] A. Y. Liu, T. Komljenovic, M. L. Davenport, A. C. Gossard, and J. E. Bowers, “Reflection sensitivity of 1.3 μm quantum dot lasers epitaxially grown on silicon,” *Opt. Express*, vol. 25, no. 9, pp. 9535–9543, 2017. doi: 10.1364/OE.25.009535.
- [101] D. Inoue et al., “Directly modulated 1.3 μm quantum dot lasers epitaxially grown on silicon,” *Opt. Express*, vol. 26, no. 6, pp. 7022–7033, 2018. doi: 10.1364/OE.26.007022.
- [102] K. Yashiki et al., “25-Gbps error-free operation of chip-scale Si-photonics optical transmitter over 70°C with integrated quantum dot laser,” in *Proc. Opt. Fiber Commun. Conf. Exhib. (OFC 2016)*, 2016, pp. Th1F–7.
- [103] K. Mizutani et al., “Isolator free optical I/O core transmitter by using quantum dot laser,” in *Proc. IEEE Int. Conf. Group IV Photon. (GFP)*, Oct. 2015, vol. 2015, pp. 177–178.
- [104] M. W. Fleming and A. Mooradian, “Spectral characteristics of external-cavity controlled semiconductor lasers,” *IEEE J. Quantum Electron.*, vol. 17, no. 1, pp. 44–59, 1981. doi: 10.1109/JQE.1981.1070634.
- [105] C. Xiang, P. A. Morton, and J. E. Bowers, “Ultra-narrow linewidth laser based on a semiconductor gain chip and extended Si₃N₄ Bragg grating,” *Opt. Lett.*, vol. 44, no. 15, pp. 3825–3828, 2019. doi: 10.1364/OL.44.003825.
- [106] H. Guan et al., “Widely-tunable, narrow-linewidth III-V/silicon hybrid external-cavity laser for coherent communication,” *Opt. Express*, vol. 26, no. 7, pp. 7920–7933, 2018. doi: 10.1364/OE.26.007920.
- [107] M. A. Tran, D. Huang, J. Guo, T. Komljenovic, P. A. Morton, and J. E. Bowers, “Ring-resonator based widely-tunable narrow-linewidth Si/InP integrated lasers,” *IEEE J. Sel. Top. Quantum Electron.*, vol. 26, no. 2, pp. 1–14, 2019. doi: 10.1109/JSTQE.2019.2935274.
- [108] C. Xiang et al., “A narrow-linewidth III-V/Si/Si₃N₄ laser using multilayer heterogeneous integration,” vol. 7, no. 1, pp. 20–21, Nov. 2019.
- [109] T. Septon et al., “Large linewidth reduction in semiconductor lasers based on atom-like gain material,” *Optica*, vol. 6, no. 8, p. 1071, 2019. doi: 10.1364/OPTICA.6.001071.
- [110] T. Septon et al., “Narrow linewidth InAs/InP quantum dot DFB laser,” in *Proc. Optical Fiber Commun. Conf. Exhib. (OFC)*, 2019, pp. 1–3.
- [111] H. Su and L. F. Lester, “Dynamic properties of quantum dot distributed feedback lasers: High speed, linewidth and chirp,” *J. Phys. D. Appl. Phys.*, vol. 38, no. 13, pp. 2112–2118, 2005. doi: 10.1088/0022-3727/38/13/006.
- [112] Y. Wan et al., “Tunable quantum dot lasers grown directly on silicon,” *Optica*, vol. 6, no. 11, p. 1394, Nov. 2019. doi: 10.1364/OPTICA.6.001394.
- [113] J.-J. He and D. Liu, “Wavelength switchable semiconductor laser using half-wave V-coupled cavities,” *Opt. Express*, vol. 16, no. 6, pp. 3896–3911, 2008. doi: 10.1364/OE.16.003896.
- [114] Y. Wan et al., “Directly modulated single-mode tunable quantum dot lasers at 1.3 μm ,” *Laser Photon. Rev.*, vol. 14, no. 3, p. 1,900,348, Mar. 2020. doi: 10.1002/lpor.201900348.
- [115] P. W. Smith, M. A. Duguay, and E. P. Ippen, “Mode-locking of lasers,” *Proc. IEEE*, vol. 58, no. 9, pp. 1342–1357, 1970. doi: 10.1109/PROC.1970.7926.
- [116] J. P. Van Der Ziel, W. T. Tsang, R. A. Logan, R. M. Mikulyak, and W. M. Augustyniak, “Subpicosecond pulses from passively mode-locked GaAs buried optical guide semiconductor lasers,” *Appl. Phys. Lett.*, vol. 39, no. 7, pp. 525–527, 1981. doi: 10.1063/1.92802.
- [117] M. G. Thompson, A. R. Rae, M. Xia, R. V. Penty, and I. H. White, “InGaAs quantum-dot mode-locked laser diodes,” *IEEE J. Sel. Top. Quantum Electron.*, vol. 15, no. 3, pp. 661–672, 2009. doi: 10.1109/JSTQE.2008.2012265.
- [118] P. Borri, W. Langbein, J. M. Hvam, F. Heinrichsdorff, M. H. Mao, and D. Bimberg, “Spectral hole-burning and carrier-heating dynamics in InGaAs quantum-dot amplifiers,” *IEEE J. Sel. Top. Quantum Electron.*, vol. 6, no. 3, pp. 544–551, 2000. doi: 10.1109/2944.865110.
- [119] D. Bimberg, M. Kuntz, and M. Laemmlin, “Quantum dot photonic devices for lightweight communication,” *Appl. Phys. A Mater. Sci. Process.*, vol. 80, no. 6, pp. 1179–1182, 2005. doi: 10.1007/s00339-004-3184-y.
- [120] D. Bimberg et al., “High speed nanophotonic devices based on quantum dots,” *Phys. Status Solidi*, vol. 203, no. 14, pp. 3523–3532, Nov. 2006. doi: 10.1002/pssa.200622488.
- [121] M. Kuntz, G. Fiol, M. Laemmlin, C. Meuer, and D. Bimberg, “High-speed mode-locked quantum-dot lasers and optical amplifiers,” *Proc. IEEE*, vol. 95, no. 9, pp. 1767–1778, Sept. 2007. doi: 10.1109/PROC.2007.900949.
- [122] S. Liu et al., “High-channel-count 20 GHz passively mode-locked quantum dot laser directly grown on Si with 41 Tbit/s transmission capacity,” *Optica*, vol. 6, no. 2, p. 128, Feb. 2019. doi: 10.1364/OPTICA.6.000128.
- [123] D. Auth, S. Liu, J. Norman, J. Edward Bowers, and S. Breuer, “Passively mode-locked semiconductor quantum dot on silicon laser with 400 Hz RF line width,” *Opt. Express*, vol. 27, no. 19, p. 27,256, Sept. 2019. doi: 10.1364/OE.27.027256.
- [124] K. Van Gasse et al., “Recent advances in the photonic integration of mode-locked laser diodes,” *IEEE Photon. Technol. Lett.*, vol. 31, no. 23, pp. 1870–1873, Oct. 2019. doi: 10.1109/LPT.2019.2945973.
- [125] G. Carpintero, M. G. Thompson, R. V. Penty, and I. H. White, “Low noise performance of passively mode-locked 10-GHz quantum-dot laser diode,” *IEEE Photon. Technol. Lett.*, vol. 21, no. 6, pp. 389–391, Mar. 2009. doi: 10.1109/LPT.2008.2001918.
- [126] P. Marin-Palomo et al., “Comb-based WDM transmission at 10 Tbit/s using a DC-driven quantum-dash mode-locked laser diode,” *Opt. Express*, vol. 27, no. 22, pp. 31,110–31,129, Apr. 2019. doi: 10.1364/OE.27.031110.
- [127] J. Sun, E. Timurdogan, A. Yaacobi, E. S. Hosseini, and M. R. Watts, “Large-scale nanophotonic phased array,” *Nature*, vol. 493, no. 7431, pp. 195–199, 2013. doi: 10.1038/nature11727.
- [128] M. L. Davenport, S. Skendzic, N. Volet, J. C. Hulme, M. J. R. Heck, and J. E. Bowers, “Heterogeneous silicon/III-V semiconductor optical amplifiers,” *IEEE J. Sel. Top. Quantum Electron.*, vol. 22, no. 6, pp. 78–88, 2016.
- [129] T. Matsumoto et al., “Hybrid-integration of SOA on silicon photonics platform based on flip-chip bonding,” *J. Light. Technol.*, vol. 37, no. 2, pp. 307–313, 2019. doi: 10.1109/JLT.2018.2870128.
- [130] P. Kaspar et al., “Hybrid III-V/silicon SOA in optical network based on advanced modulation formats,” *IEEE Photonics Technol. Lett.*, vol. 27, no. 22, pp. 2383–2386, Nov. 2015. doi: 10.1109/LPT.2015.2466543.
- [131] K. Van Gasse, R. Wang, and G. Roelkens, “27 dB gain III–V-on-silicon semiconductor optical amplifier with >17 dBm output power,” *Opt. Express*, vol. 27, no. 1, pp. 293–302, 2019. doi: 10.1364/OE.27.000293.
- [132] S. Cheung, Y. Kawakita, K. Shang, and S. J. Ben Yoo, “Highly efficient chip-scale III-V/silicon hybrid optical amplifiers,” *Opt. Express*, vol. 23, no. 17, pp. 22,431–22,443, 2015. doi: 10.1364/OE.23.022431.
- [133] R. Jones et al., “Heterogeneously integrated InP/Silicon photonics: Fabricating fully functional transceivers,” *IEEE Nanotechnol. Mag.*, vol. 13, no. 2, pp. 17–26, 2019. doi: 10.1109/MNANO.2019.2891369.
- [134] T. W. Berg, J. Mork, and J. M. Hvam, “Gain dynamics and saturation in semiconductor quantum dot amplifiers,” *New J. Phys.*, vol. 6, no. 1, pp. 1–23, 2004. doi: 10.1088/1367-2630/6/1/178.